Available online at www.sciencedirect.com
SCIENCE DIRECT
Planetary and Space Science 54 (2006) 932–956
Planetary and Space Science
www.elsevier.com/locate/pss

Five years of Ulysses dust data: 2000–2004

H. Krüger[a,*], N. Altobelli[b], B. Anweiler[c], S.F. Dermott[d], V. Dikarev[c], A.L. Graps[e], E. Grün[c,f], B.A. Gustafson[d], D.P. Hamilton[g], M.S. Hanner[b], M. Horányi[h], J. Kissel[a], M. Landgraf[i], B.A. Lindblad[j], D. Linkert[c], G. Linkert[c], I. Mann[k], J.A.M. McDonnell[l], G.E. Morfill[m], C. Polanskey[b], G. Schwehm[n], R. Srama[c], H.A. Zook[o,✠]

[a]*Max-Planck-Institut für Sonnensystemforschung, 37191 Katlenburg-Lindau, Germany*
[b]*Jet Propulsion Laboratory, Pasadena, CA 91109, USA*
[c]*Max-Planck-Institut für Kernphysik, 69029 Heidelberg, Germany*
[d]*University of Florida, 211 SSRB, Campus, Gainesville, FL 32609, USA*
[e]*INAF-Istituto di Fisica dello Spazio Interplanetario, CNR - ARTOV, 00133 Roma, Italy*
[f]*Hawaii Institute of Geophysics and Planetology, Honolulu, HI 96822, USA*
[g]*University of Maryland, College Park, MD 20742-2421, USA*
[h]*Laboratory for Atmospheric and Space Physics, University of Colorado, Boulder, & CO 80309, USA*
[i]*ESOC, 64293 Darmstadt, Germany*
[j]*Lund Observatory, 221 Lund, Sweden*
[k]*Institut für Planetologie, Universität Münster, 48149 Münster, Germany*
[l]*Planetary and Space Science Research Institute, The Open University, Milton Keynes, MK7 6AA, UK*
[m]*Max-Planck-Institut für Extraterrestrische Physik, 85748 Garching, Germany*
[n]*ESTEC, 2200 AG Noordwijk, The Netherlands*
[o]*NASA Johnson Space Center, Houston, TX 77058, USA*

Received 20 December 2005; received in revised form 25 April 2006; accepted 25 April 2006
Available online 27 June 2006

Abstract

The Ulysses spacecraft has been orbiting the Sun on a highly inclined ellipse ($i = 79^\circ$, perihelion distance 1.3 AU, aphelion distance 5.4 AU) since it encountered Jupiter in 1992. Between January 2000 and December 2004, the spacecraft completed almost an entire revolution about the Sun, passing through perihelion in May 2001 and aphelion in July 2004. In this five-year period the dust detector on board recorded 4415 dust impacts. We publish and analyse the complete data set of both raw and reduced data for particles with masses $10^{-16}\,\mathrm{g} \leqslant m \leqslant 10^{-7}\,\mathrm{g}$. Together with 1695 dust impacts recorded between launch of Ulysses and the end of 1999 published earlier (Grün, E., Baguhl, M., Divine, N., Fechtig, H., Hamilton, D.P, Hanner, M.S., Kissel, J., Lindblad, B.A., Linkert, D., Linkert, G., Mann, I., McDonnell, J.A.M., Morfill, G.E., Polanskey, C., Riemann, R., Schwehm, G.H., Siddique, N., Staubach, P., Zook, H.A., 1995a. Two years of Ulysses dust data. Planetary Space Sci. 43, 971–999, Paper III; Krüger, H., Grün, E., Landgraf, M., Baguhl, M., Dermott, S.F., Fechtig, H., Gustafson, B.A., Hamilton, D.P., Hanner, M.S., Horányi, M., Kissel, J., Lindblad, B., Linkert, D., Linkert, G., Mann, I., McDonnell, J.A.M., Morfill, G.E., Polanskey, C., Schwehm, G.H., Srama, R., Zook, H.A., 1995. Three years of Ulysses dust data: 1993 to 1995. Planetary and Space Sci. 47, 363–383, Paper V; Krüger, H., Grün, E., Landgraf, M., Dermott, S.F., Fechtig, H., Gustafson, B.A., Hamilton, D.P., Hanner, M.S., Horányi, M., Kissel, J., Lindblad, B., Linkert, D., Linkert, G., Mann, I., McDonnell, J.A.M., Morfill, G.E., Polanskey, C., Schwehm, G.H., Srama, R., Zook, H.A., 2001b. Four years of Ulysses dust data: 1996 to 1999. Planetary Space Sci. 49, 1303–1324, Paper VII), a data set of 6110 dust impacts detected with the Ulysses sensor between October 1990 and December 2004 is now available. The impact rate measured between 2000 and 2002 was relatively constant with about 0.3 impacts per day showing a maximum at 1.5 per day around ecliptic plane crossing in early-2001. The impact direction of the majority of impacts between 2000 and 2002 is compatible with particles of interstellar origin, the rest are most likely interplanetary particles. In 2003 and 2004 dust stream particles originating from the jovian system dominated the overall impact rate. Twenty-two individual dust streams were measured between November 2002 and December 2004. The observed impact rates are compared with models for interplanetary

*Corresponding author.
E-mail address: krueger@mps.mpg.de (H. Krüger).
✠Deceased 2001.

0032-0633/$ - see front matter
doi:10.1016/j.pss.2006.04.015

and interstellar dust. The dust measurements from the entire mission since Ulysses launch give good agreement with the interplanetary flux model of Staubach, P., Grün, E., Jehn, R., 1997. The meteoroid environment near Earth, Adv. Space Res. 19, 301–308.

Keywords: Interplanetary dust; Interstellar dust; Dust streams; Lorentz force; Jupiter dust; Zodiacal dust

1. Introduction

The Ulysses spacecraft was launched in 1990 and is the first spaceprobe to reach high ecliptic latitudes. The craft's orbital plane is almost perpendicular to the ecliptic plane with an aphelion at Jupiter. Ulysses is equipped with a highly sensitive impact ionisation dust detector which measures impacts of micrometre and sub-micrometre dust grains. The detector is practically identical with the dust instrument which flew on board the Galileo spaceprobe. Both instruments were described in previous publications (Grün et al., 1992a,b, 1995c).

Ulysses and Galileo dust measurements have been used to study the three-dimensional distribution of the interplanetary dust complex and their relation to the underlying populations of parent bodies like asteroids and comets (Divine, 1993; Grün et al., 1997; Staubach et al., 1997). Studies of asteroidal dust released from the IRAS dust bands show that they are not efficient enough dust sources to maintain a stable interplanetary dust cloud (Mann et al., 1996). The state of the inner solar system dust cloud within approximately 1 AU from the Sun including dust destruction and ion formation processes in relation to so-called solar wind pickup ions detected by the Solar Wind Ion Composition Spectrometer onboard Ulysses was recently investigated (Mann et al., 2004; Mann and Czechowski, 2005). An improved physical model was developed for the interplanetary meteoroid environment (Dikarev et al., 2001, 2002) which uses long-term particle dynamics to define individual interplanetary dust populations. The Ulysses and Galileo in situ dust data are an important data set for the validation of this model. The properties of β-meteoroids (i.e. dust particles which leave the solar system on unbound orbits due to acceleration by radiation pressure) were also studied with the Ulysses data set (Wehry and Mann, 1999; Wehry et al., 2004). Finally, the potential connection of cometary dust trails and enhancements of the interplanetary magnetic field as measured by Ulysses was investigated by Jones and Balogh (2003).

The Ulysses dust instrument discovered burst-like intermittent streams of tiny dust grains in interplanetary space (Grün et al., 1993) which had been emitted from the jovian system (Zook et al., 1996). This discovery was completely unexpected and no periodic phenomenon for tiny dust grains in interplanetary space was known before. These grains strongly interacted with the interplanetary and the jovian magnetic fields (Hamilton and Burns, 1993; Horányi et al., 1993, 1997; Grün et al., 1998) and the majority of them originated from Jupiter's moon Io (Graps et al., 2000). In February 2004 Ulysses had its second Jupiter flyby (at 0.8 AU distance from the planet) and again measured the jovian dust streams (Krüger et al., 2005a, 2006b).

Another important discovery of the Ulysses detector were interstellar dust particles sweeping through the heliosphere (Grün et al., 1993). The grains which originated from the local interstellar cloud (LIC) were identified by their impact direction and impact velocities, the latter being compatible with particles moving on hyperbolic heliocentric trajectories (Grün et al., 1994). Their dynamics depends on the grain size and is strongly affected by the interaction with the interplanetary magnetic field and by solar radiation pressure (Mann and Kimura, 2000; Landgraf, 2000; Czechowski and Mann, 2003). As a result the size distribution and fluxes of grains measured inside the heliosphere are strongly modified (Landgraf et al., 1999, 2003). The intrinsic size distribution of interstellar grains in the LIC extends to grain sizes larger than those detectable by astronomical observations (Frisch et al., 1999; Frisch and Slavin, 2003; Landgraf et al., 2000; Grün and Landgraf, 2000). The existence of such 'big' interstellar grains is also indicated by observations of radar meteors entering the Earth's atmosphere (Taylor et al., 1996; Baggaley and Neslusan, 2002). The Ulysses measurements showed that the dust-to-gas mass ratio in the local interstellar cloud is several times higher than the standard interstellar value derived from cosmic abundances, implying the existence of inhomogeneities in the diffuse interstellar medium on relatively small length scales. Finally, previous analyses may have overestimated by about 20% the interstellar dust flux and the velocity dispersion of the interstellar dust stream by about 30%, respectively, due to neglect of the inner sensor side wall which turned out to have a similar sensitivity to dust impacts as the detector target itself (Altobelli et al., 2004; Willis et al., 2005).

Comprehensive reviews of the scientific achievements of the Ulysses mission including results from the dust investigation were given by Balogh et al. (2001) and Grün et al. (2001). References to other works related to Ulysses and Galileo measurements on dust in the planetary system were also given by Grün et al. (1995a,b) and Krüger et al. (1999a,b,2001a,b).

This is the ninth paper in a series dedicated to presenting both raw and reduced data obtained from the dust instruments on board the Ulysses and Galileo spacecraft. The reduction process of Ulysses and Galileo dust data was described by Grün et al. (1995c, hereafter Paper I). In Papers III,V and VII (Grün et al., 1995a; Krüger et al., 1999b, 2001b) we present the Ulysses data set spanning the

time period from launch in October 1990 to December 1999. Papers II, IV and VI (Grün et al., 1995b; Krüger et al., 1999a, 2001a) discuss the seven years of Galileo data from October 1989 to December 1996. The current paper extends the Ulysses data set from January 2000 until December 2004, and a companion paper (Krüger et al., 2006a, Paper VIII) presents Galileo's 1997–1999 measurements around Jupiter.

The main data products are a table of the impact rate of all impacts determined from the particle accumulators and a table of both raw and reduced data of all dust impacts for which the full data set of measured impact parameters was transmitted to Earth. The information presented in these papers is similar to data which we are submitting to the various data archiving centres (Planetary Data System, NSSDC, Ulysses Data Centre). Electronic access to the data is also possible via the world wide web: http://www.mpi-hd.mpg.de/dustgroup/.

This paper is organised like Papers III,V and VII. We begin with an overview of important events of the Ulysses mission between 2000 and 2004 (Section 2). Sections 3 and 4 describe and analyse the Ulysses dust data set for this period. In Section 5 we discuss the properties of different populations of interplanetary and interstellar dust in the data set and compare our recent measurements of the jovian dust streams with those obtained during the first Jupiter flyby in 1992. In Section 6 we summarise our conclusions.

2. Mission and instrument operation

2.1. Ulysses mission and dust instrument characteristics

The Ulysses spacecraft was launched on 6 October 1990. A swing-by manoeuvre at Jupiter in February 1992 rotated the orbital plane 79° relative to the ecliptic plane. On the resulting trajectory (Fig. 1) Ulysses finished two full revolutions about the Sun. Passages over the south pole of the Sun occurred in October 1994 and November 2000, passages through the ecliptic plane at a perihelion distance of 1.3 AU occurred in March 1995 and May 2001, and passes over the Sun's north pole were in August 1995 and October 2001. In April 1998 and July 2004, the spacecraft crossed the ecliptic plane at an aphelion distance of 5.4 AU. In 2007/08 Ulysses will make its third pass over the Sun's polar regions. Orbital elements for the out-of-ecliptic part of the Ulysses trajectory are given in Paper VII. Fig. 1 shows that during the time interval considered in this paper Ulysses completed almost an entire revolution about the Sun.

Ulysses spins at five revolutions per minute about the centre line of its high gain antenna which normally points at Earth. Fig. 2 shows the deviation of the spin axis from the Earth direction for the period 2000–2004. Most of the time the spin axis pointing was within 0.5° of the nominal Earth direction, similar to the mission before 2000. This small deviation is usually negligible for the analysis of measurements with the dust detector. The Ulysses spacecraft and mission are explained in more detail by Wenzel et al. (1992). Details about the data transmission to Earth can also be found in Paper III.

The Ulysses dust detector (GRU) has a 140° wide field of view and is mounted at the spacecraft nearly at right angles (85°) to the antenna axis (spacecraft spin axis). Due to this mounting geometry, the dust sensor is most sensitive to particles approaching from the plane perpendicular to the spacecraft–Earth direction. The impact direction of dust particles is measured by the rotation angle which is the sensor-viewing direction at the time of a dust impact. During one spin revolution of the spacecraft the rotation

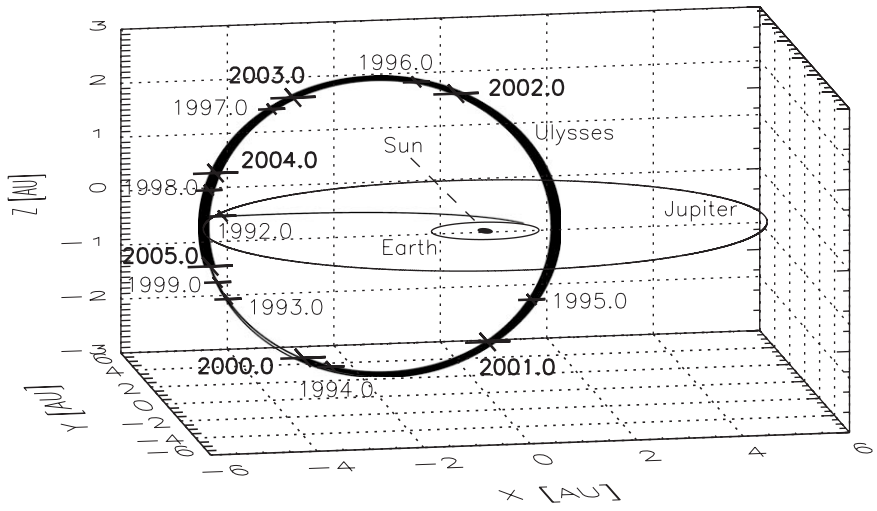

Fig. 1. The trajectory of Ulysses in ecliptic coordinates. The Sun is in the centre. The orbits of Earth and Jupiter indicate the ecliptic plane. The initial trajectory of Ulysses was in the ecliptic plane. Since Jupiter flyby in early-1992 the orbit has been almost perpendicular to the ecliptic plane (79° inclination). Crosses mark the spacecraft position at the beginning of each year. The 2000–2004 part of the trajectory is shown as a thick line. Vernal equinox is to the right (positive x-axis).

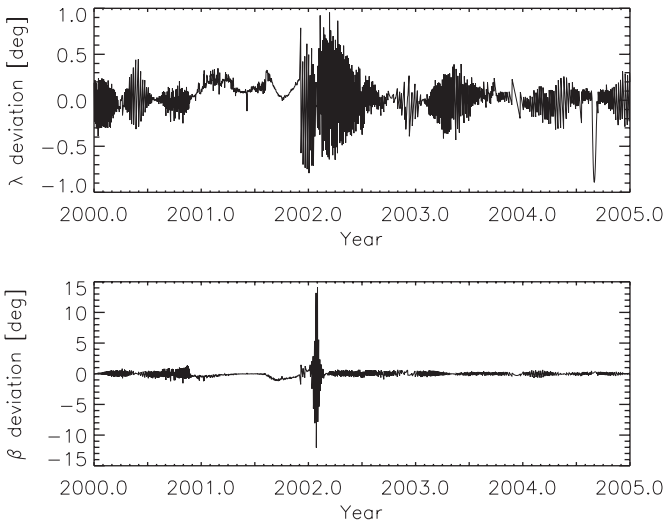

Fig. 2. Spacecraft attitude: deviation of the antenna pointing direction (i.e. positive spin axis) from the nominal Earth direction. The angles are given in ecliptic longitude (top) and latitude (bottom, equinox 1950.0).

angle scans through a complete circle of 360°. Zero degrees rotation angle is defined to be the direction closest to ecliptic north. At high ecliptic latitudes, however, the sensor pointing at 0° rotation angle significantly deviates from the actual north direction. During the passages over the Sun's polar regions the sensor always scans through a plane tilted by about 30° from the ecliptic plane and all rotation angles lie close to the ecliptic plane (cf. Fig. 4 in Grün et al., 1997). A sketch of the viewing geometry around aphelion passage can be found in Grün et al. (1993).

The available electrical power on board Ulysses became an issue beginning in 2001 due to decreasing power generation of the radioisotope batteries (RTGs). Some instrument heaters on board had to be switched off to save power which in turn also reduced the on board temperature. Later, in 2002, power consumption could not be sufficiently reduced anymore by simply switching off heaters and a cycling instrument operation scheme had to be implemented: one or more of the scientific instruments had to be switched off at a time. The dust instrument had to be switched off only once, namely from December 2002 through May 2003.

2.2. Dust instrument operation

Table 1 gives significant mission and dust instrument events from 2000 to 2004. Earlier events are only listed if especially significant. A comprehensive list of events from launch until the end of 1999 was given in Papers III, V and VII.

On 27 June 2000 a spacecraft anomaly occurred during which all scientific instruments on board Ulysses were switched off automatically. This disconnection of all non-essential loads is called DNEL for short. Within about two days after the DNEL, the dust instrument was switched on again and reconfigured to its nominal operational mode. The resulting loss of continuous measurement time with the dust instrument is negligible. Between 1 December 2002 and 3 June 2003 the dust instrument was switched off because there was not enough electrical power anymore to operate all instruments simultaneously.

The dust instrument has two heaters to allow for a relatively stable operating temperature within the sensor. By heating one of the two or both heaters, three different heating power levels can be achieved (0.4, 0.8 or 1.2 W; for comparison, the total power consumption of the instrument without heaters is 2.2 W). Sensor heating was necessary when the spacecraft was outside about 2 AU because relatively little radiation was received from the Sun.

Before 2001 one or both heaters were switched on beyond 2 AU, except close to the Sun when both were switched off. Since November 2001, the maximum allowed heating power for nominal dust instrument operation has been limited to 0.8 W to save power on board Ulysses. This reduced the sensor temperature by about 10 °C as compared to the configuration with 1.2 W heating power at similar heliocentric distance. The full heating power is only allowed for short periods before instrument switch on to avoid damage of the electronics. It should be noted that during DNELs the heaters were switched off, but switched on again several hours before the instrument was reconfigured so that a stable operating temperature could be achieved at switch on.

Table 1 lists the total powers consumed by the heaters. From 2000 to 2004, the temperature of the dust sensor was between +12 and −37 °C. The lower limit for the specified operational range is −30 °C. No major effect of the lower temperature was recognised. The only anomaly seen so far was a flipping in the housekeeping value of the channeltron high voltage between days 184 and 192 in 2004 which was coincident with a temperature drop in the electronics box from 4.5 to 0.5 °C. The flipping was caused by an unstable operational condition at this temperature of the analogue-to-digital converter to which the channeltron is connected. It was not caused by a real fluctuation of the channeltron high voltage.

On 26 March 2002 the Ulysses dust instrument was reprogrammed for the first time since 1993 (Paper V) and restarted in its nominal configuration on 8 April 2002. A new classification scheme for impact events was implemented. It is the same as the one installed in the Galileo instrument in July 1994 which is described in detail in Paper IV.

On 28 July 2003 an attempt was made to reprogram the instrument once again to extend the time word (TIME, see Paper I). However, due to an error in the program, this reprogramming failed and after a few unsuccessful attempts the old program (i.e. the one loaded in March 2002) had to be started on 22 August 2003. Unfortunately, due to this unsuccessful attempt, no dust measurements

Table 1
Ulysses mission and dust detector (GRU) configuration, tests and other events

Yr-day	Date	Time	Event
90-279	06.10.90		Ulysses launch
95-300	27.10.95	16:23	GRU heater: 1,200 mW
99-048	17.02.99	04:29	GRU nominal configuration: HV = 3, EVD = C,I, SSEN = 0001
00-006	06.01.00	12:00	GRU noise test
00-034	03.02.00	09:00	GRU noise test
00-062	02.03.00	09:00	GRU noise test
00-091	31.03.00	10:00	GRU noise test
00-118	27.04.00	06:00	GRU noise test
00-146	25.05.00	06:00	GRU noise test
00-175	23.06.00	05:00	GRU noise test
00-179	27.06.00	04:04	DNEL # 10, GRU off
00-179	27.06.00	13:19	GRU on
00-181	29.06.00	05:57	GRU nominal configuration
00-202	20.07.00	00:00	GRU noise test
00-230	17.08.00	00:00	GRU noise test
00-242	29.08.00	22:52	GRU HV = 4
00-265	21.09.00	17:30	GRU heater: 800 mW
00-265	21.09.00	18:00	GRU noise test
00-294	20.10.00	18:00	GRU noise test
00-321	16.11.00	01:00	GRU noise test
00-332	27.11.00		Ulysses maximum south solar latitude (−80.2°)
00-349	14.12.00	01:00	GRU noise test
01-011	11.01.01	01:00	GRU noise test
01-039	08.02.01	01:00	GRU noise test
01-047	16.02.01	19:30	GRU heater: 400 mW
01-067	08.03.01	00:00	GRU noise test
01-095	05.04.01	01:00	GRU noise test
01-097	07.04.01	18:15	GRU heater: off
01-123	03.05.01	01:00	GRU noise test
01-137	17.05.01	15:12	GRU HV = 3, EVD = C,I, SSEN = 0011
01-143	23.05.01		Ulysses perihelion passage (1.34 AU)
01-145	25.05.01		Ulysses ecliptic plane crossing
01-151	31.05.01	19:00	GRU noise test
01-179	28.06.01	19:00	GRU noise test
01-207	26.07.01	19:00	GRU noise test
01-235	23.08.01	19:00	GRU noise test
01-263	20.09.01	19:00	GRU noise test
01-274	01.10.01	15:15	GRU new nominal configuration: HV = 4, EVD = C,I, SSEN = 0001
01-274	01.10.01	15:25	GRU heater: 400 mW
01-287	13.10.01		Ulysses maximum north solar latitude (+80.2°)
01-291	18.10.01	06:00	GRU noise test
01-312	08.11.01	17:40	URAP sounder off
01-319	15.11.01	06:00	GRU noise test
01-325	21.11.01	18:25	GRU heater: 800 mW
01-347	13.12.01	04:00	GRU noise test
02-010	10.01.02	18:00	GRU noise test
02-037	06.02.02	14:00	GRU noise test
02-066	07.03.02	10:00	GRU noise test
02-085	26.03.02	02:26	GRU reprogramming,new onboard classification scheme
02-098	08.04.02	15:33	GRU start new program
02-098	08.04.02	15:44	GRU nominal configuration
02-121	01.05.02	11:00	GRU noise test
02-149	29.05.02	11:00	GRU noise test
02-176	25.06.02	22:00	GRU noise test
02-206	25.07.02	23:00	GRU noise test
02-234	22.08.02	10:00	GRU noise test
02-262	19.09.02	15:00	GRU noise test
02-291	18.10.02	19:00	GRU noise test
02-318	14.11.02	18:00	GRU noise test
02-335	01.12.02	04:37	GRU off (for onboard power-sharing)
03-152	01.06.03	02:42	GRU heater: 1,200 mW
03-154	03.06.03	03:38	GRU heater: 800 mW
03-154	03.06.03	03:39	GRU on

Table 1 (*continued*)

Yr-day	Date	Time	Event
03-155	04.06.03	04:23	GRU nominal configuration
03-177	26.06.03	00:00	GRU noise test
03-205	24.07.03	00:00	GRU noise test
03-209	28.07.03	09:26	GRU unsuccessful reprogramming attempt to increase time word
03-229	17.08.03	20:55	GRU activation of old program
03-234	22.08.03	17:39	GRU nominal configuration
03-261	18.09.03	13:00	GRU noise test
03-288	15.10.03	12:00	GRU noise test
03-317	13.11.03	14:00	GRU noise test
03-323	19.11.03		Ulysses maximum jovicentric latitude (75.5°)
03-345	11.12.03	08:30	GRU noise test
04-008	08.01.04	11:00	GRU noise test
04-035	04.02.04		Ulysses distant Jupiter encounter (0.80 AU or 1684 R_J)
04-037	06.02.04	09:00	GRU noise test
04-064	04.03.04	01:00	GRU noise test
04-092	01.04.04	04:00	GRU noise test
04-120	29.04.04	04:00	GRU noise test
04-148	27.05.04	03:00	GRU noise test
04-176	24.06.04	02:00	GRU noise test
04-182	30.06.04		Ulysses aphelion passage (5.4 AU)
04-196	14.07.04		Ulysses ecliptic plane crossing
04-204	22.07.04	04:00	GRU noise test
04-232	19.08.04	18:00	GRU noise test
04-261	17.09.04	13:00	GRU noise test
04-289	15.10.04	13:00	GRU noise test
04-318	13.11.04	11:00	GRU noise test
04-335	30.11.04	10:25	GRU new program load (increased time word)
03-337	02.12.04	11:00	GRU start new program nominal configuration
04-344	09.12.04	09:50	GRU noise test

Only selected events are given before 2000.See Section 2 for details. Abbreviations used: DNEL: Disconnect non-essential loads (i.e. all scientific instruments); HV: channeltron high voltage step; EVD: event definition, ion—(I), channeltron—(C), or electron-channel (E); SSEN: detection thresholds, ICP, CCP, ECP and PCP.

Times when no data could be collected with the dust instrument: 26 March–8 April 2002, 1 December 2002–3 June 2003, 28 June–22 August 2003 and 30 November–2 December 2004.

could be collected during almost 4 weeks. Another attempt on 30 November 2004 was successful and the new program was started on 2 December 2004. Since then the TIME increment can be set between 5.6 min and 255 days. The TIME word was set to a default value of 1 h so that a time range of 255 h $\simeq$ 10.5 days is covered before it is reset to zero. Up to now, the TIME word is not used for data analysis. The TIME word may become relevant for determination of the impact time in the future in case long periods without data transmission from Ulysses to the Earth have to be covered.

2.3. Instrument sensitivity and noise

Analysis of the in-orbit noise characteristics of the dust instrument (Paper III) led to a relatively noise-free configuration with which the instrument was normally operated before 2000: channeltron voltage 1140 V (HV = 3); event definition status such that either the channeltron or the ion-collector channel can, independent of each other, start a measurement cycle (EVD = C, I); detection thresholds for ion-collector, channeltron and electron-channel set to the lowest levels and the detection threshold for the entrance grid set to the first digital step (SSEN = 0, 0, 0, 1). See Paper I for a description of these terms. This instrument set-up was the nominal configuration before 2000.

In order to monitor instrument health and noise characteristics, dedicated noise tests were performed at monthly intervals. During all these tests the operational setting was changed in four steps at 1-h intervals, starting from the nominal configuration described above: (a) set the event definition status such that the channelton, the ion-collector and the electron-channel can initiate a measurement cycle (EVD = C, I, E); (b) set the thresholds for all channels to their lowest levels (SSEN = 0, 0, 0, 0); (c) reset the event definition status to its nominal configuration (EVD = C, I) and increase the channeltron high voltage by one step with respect to the nominal configuration; (d) reset the instrument to its nominal configuration (i.e. reduce the channeltron high voltage by one step and set the detection thresholds to SSEN = 0, 0, 0, 1).

The noise tests performed before 2000 revealed a long-term drop in the noise sensitivity of the instrument (Paper VII): in step (c), when the channeltron high voltage was raised, fewer noise events were triggered compared to

the beginning of the mission. This was most likely caused by a reduction in the channeltron amplification due to ageing. To counterbalance the reduced amplification we increased the channeltron high voltage by one digital step on 29 August 2000 (HV = 4, 1240 V). This raised the instrument sensitivity close to its original value from the earlier mission. Although the ageing of the channeltron led to a drop in the number of class 3 impacts, dust impacts which would have triggered class 3 events should have shown up in lower quality classes. The noise response of the Ulysses dust detector will be monitored in the future to maintain stable instrument operation.

In step (c) of the noise test, i.e. when the channeltron high voltage was raised by one digital step w.r.t. the nominal value, the noise signals usually showed a channeltron charge amplitude CA = 1 (digital units) between 1991 and 1996. Beginning in 1997 values of CA = 0 occurred frequently which was also indicative of a channeltron degradation (Paper VII). Since August 2000, when the nominal channeltron high voltage was raised, CA = 0 has almost disappeared and values of CA = 1 dominate again, confirming that the increase in the channeltron voltage has raised the channeltron amplification as intended.

On 17 May 2001 we had to reduce the channeltron voltage to its former value because strong solar activity caused an elevated noise rate. HV = 3 was again the nominal setting until 1 October 2001 when the solar activity had dropped. Since 1 October 2001 HV = 4 has been the nominal channeltron high voltage setting again. Note that during noise tests the channeltron voltage was always raised by one digital step (i.e. to HV = 5 since 1 October 2001).

In addition to the reduction of the channeltron high voltage, the detection threshold for the electron-channel was raised by one digital step (to 2.6×10^{-14} C) between 17 May and 1 October 2001 (i.e. days 01–137 and 01–274) to reduce the noise sensitivity. Even though these settings should have reduced the noise sensitivity, coincidences between the electron signal and the channeltron signal could still have occurred by chance. Thus, noise events could have the signal characteristics of dust impacts with low electron charges. Therefore, two impacts in the lowest ion amplitude range AR1 (# 1972 and 2063 on days 01–146 and 01–274, respectively) with electron charge amplitudes EA = 1 or 2 should be treated with caution (see Section 3 and Paper I for further explanation of these instrument parameters).

Fig. 3 shows the noise rate of the dust instrument for the 2000–2004 period. The upper panel shows the daily maxima of the noise rate. Before 8 November 2001 the daily maxima were dominated by noise due to interference with the sounder of the Unified RAdio and Plasma wave instrument (URAP) on board Ulysses (Stone et al., 1992). The sounder was typically operated for periods of only 2 min with quiet intervals of about 2 h. Thus, the high noise rates caused by the sounder occurred only during about

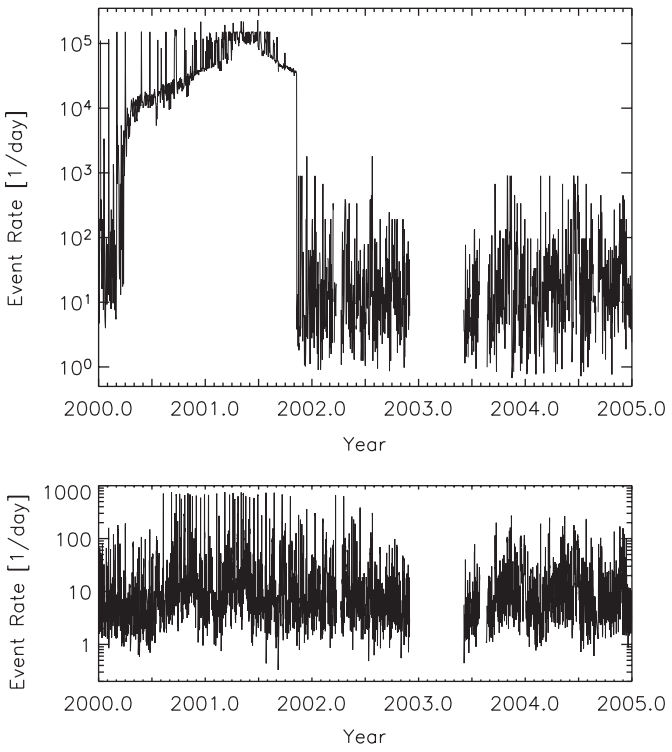

Fig. 3. Noise rate (class 0 events) detected with the dust instrument. Upper panel: daily maxima in the noise rate (determined from the AC01 accumulator). Before 8 November 2001, the sounder was operated for 2% of the total time, and the daily maxima are dominated by sounder noise. After 8 November 2001 the sounder was switched off permanently. Sharp spikes are caused by periodic noise tests or short periods of reconfiguration after DNELs (Table 1). Lower panel: noise rate detected during quiet intervals when the sounder was switched off, which was the case about 98 % of the time before 8 November 2001 and 100% later. The curve shows a one-day average calculated from the number of AC01 events for which the complete information was transmitted to Earth.

2% of the total time. The remaining 98% were free of sounder noise. The sounder noise was sufficiently high to cause significant dead time in the dust instrument during the time intervals of sounder operation.

The noise rates measured during sounder operation were correlated with the distance to, and the position of, the Sun with respect to the sensor-viewing direction (Baguhl et al., 1993). Most noise events were triggered when the Sun shone directly into the sensor. Strong sounder noise occurred in 2000 and 2001 while Ulysses was within about 3 AU heliocentric distance similar to earlier periods at comparable distance (Paper V). This continued until 8 November 2001 when the sounder was switched off permanently for power saving (Fig. 3, upper panel).

When the spacecraft was at a large heliocentric distance, the noise rate was very low even during periods of sounder operation. This was the case before February 2000 (see also Papers V and VII). In 2000, the maxima in the noise rate induced by the sounder began to increase significantly when Ulysses approached the inner solar system and the

highest noise rates occurred around perihelion passage in May 2001. When the sounder was switched off permanently in November 2001 the noise rate dropped by more than 3 orders of magnitude to about 10 events per day. Individual sharp spikes in the upper panel of Fig. 3 are caused by noise tests which occurred at monthly intervals.

The noise rates when the sounder was switched off are shown in the lower panel of Fig. 3. The average was about 10 events per day and this was random noise not related to the sounder. Dead time is negligible during these periods. These noise rates are very similar to those measured during the earlier mission before 2000 showing that the overall instrument degradation was small during the entire mission. Note that the noise rate noticeably increased in August 2000 when the channeltron voltage was raised by one digital step.

3. Impact events

The dust instrument classifies all impact events into four classes and six ion charge amplitude ranges which leads to 24 individual categories. In addition, the instrument has 24 accumulators with one accumulator belonging to one individual category. Class 3, our highest class, are real dust impacts and class 0 are mostly noise events. Depending upon the noise of the charge measurements, classes 1 and 2 can be true dust impacts or noise events. This classification scheme for impact events was described in Paper I and it was valid for the Ulysses dust instrument from launch until 26 March 2002 when the instrument was reprogrammed (Table 1). Since then the classification scheme has been the same as the one used in the Galileo instrument (Paper IV).

Between 1 January 2000 and 31 December 2004, the complete data sets (sensor orientation, charge amplitudes, charge rise times, etc.) of 50 878 events including 4415 dust impacts were transmitted to Earth. Table 2 lists the number of all dust impacts counted with the 24 accumulators of the instrument. 'ACxy' refers to class number 'x' and amplitude range 'y' (for a detailed description of the accumulator categories see Paper I). As discussed in the previous section, most noise events were recorded during the short time periods when either the sounder of the URAP instrument was operating (Paper III) or when the dust instrument was configured to its high sensitive state for noise tests, or both. During these periods many events were only counted by one of the 24 accumulators because their full information was overwritten before the data could be transmitted to Earth. Since the dust impact rate was low during times outside these periods, it is expected that only the data sets of very few true dust impacts were lost.

Throughout this paper we call all particles in amplitude ranges 2 and higher (AR2–AR6) 'big'. Particles in the lowest amplitude range (AR1) are called 'small'. Before 2002 the small particles were mostly detected over the Sun's poles. After the re-occurrence of the jovian dust streams at the end of 2002 the small particles were dominated by jovian stream particles. During the entire five-year period the big particles were mostly of interplanetary and interstellar origin (Fig. 9, see also Papers III, V and VII for the earlier time periods). A few dust streams, however, also contained a small number of bigger grains in AR2. Note that these terms 'small' and 'big' do *not* have the same meaning as in Paper II and in Baguhl et al. (1993).

Table 3 lists all 290 particles detected in AR2–AR6 between January 2000 and December 2004 for which the complete information exists. We do not list the small particles (AR1) because the majority of them are jovian stream particles whose masses and velocities are outside the calibrated range of the dust instrument. The stream particles are about 10 nm in size and their velocities exceed 200 km s^{-1} (Zook et al., 1996) and any mass and velocity calibration would be unreliable. The complete information of a total of 4125 small particles was transmitted to Earth from 2000 to 2004. The full data set of all 4415 particles is available in electronic form.

In Table 3 dust particles are identified by their sequence number and their impact time. Gaps in the sequence number are due to the omission of the small particles. The event categories—class (CLN) and amplitude range (AR)—are given. Raw data as transmitted to Earth are displayed in the next columns: sector value (SEC) which is the spacecraft spin orientation at the time of impact, impact charge numbers (IA, EA, CA) and rise times (IT, ET), time difference and coincidence of electron and ion signals (EIT, EIC), coincidence of ion and channeltron signal (IIC), charge reading at the entrance grid (PA) and time (PET) between this signal and the impact. Then the instrument configuration is given: event definition (EVD), charge sensing thresholds (ICP, ECP, CCP, PCP) and channeltron high voltage step (HV). See Paper I for further explanation of the instrument parameters.

The next four columns in Table 3 give information about Ulysses' orbit: heliocentric distance (R), ecliptic longitude and latitude (LON, LAT) and distance from Jupiter (D_{Jup}, in jovian radii $R_{\mathrm{J}} = 71\,492$ km). The next column gives the rotation angle (ROT) as described in Section 2. Then follows the pointing direction of the dust instrument at the time of particle impact in ecliptic longitude and latitude (S_{LON}, S_{LAT}). Mean impact velocity (v, in km s^{-1}) and velocity error factor (VEF, i.e. multiply or divide stated velocity by VEF to obtain upper or lower limits) as well as mean particle mass (m, in grams) and mass error factor (MEF) are given in the last columns. For VEF > 6, both velocity and mass values should be discarded. This occurs for one impact in AR2–AR6. No intrinsic dust charge values are given (Svestka et al., 1996, see for a detailed analysis). Recently, reliable charge measurements for interplanetary dust grains were reported for the Cassini dust detector (Kempf et al., 2004). These measurements may lead to an improved understanding of the charge measurements of Ulysses and Galileo in the future.

Table 2
Overview of dust impacts detected with the Ulysses dust detector between 1 January 2000 and 31 December 2004 as derived from the accumulators[a]

Date	Time	R(AU)	Δt (d)	AC 01[a]	AC 11[a]	AC 21	AC 31	AC 02[a]	AC 12	AC 22	AC 32	AC 03	AC 13	AC 23	AC 33	AC 04	AC 14	AC 24	AC 34	AC 05	AC 15	AC 25	AC 35	AC 06	AC 16	AC 26	AC 36
00-001	06:10	4.160	5.333	1	-	-	-	-	-	-	-	-	-	-	-	-	-	-	-	-	-	-	-	-	-	-	-
00-046	15:36	3.960	45.39	2	-	-	2	2	1	-	-	-	-	-	3	-	-	-	-	-	-	-	-	-	-	-	-
00-070	09:10	3.850	23.73	2	-	-	-	-	-	-	1	1	-	-	-	-	-	-	-	-	-	-	-	-	-	-	-
00-108	03:23	3.660	37.75	8	-	-	-	-	1	-	-	-	-	-	1	-	-	-	-	-	-	-	-	-	-	-	-
00-129	01:24	3.550	20.91	5	1	-	-	-	-	-	-	-	-	-	-	-	-	-	-	-	-	-	-	-	-	-	-
00-175	07:49	3.290	46.26	3	-	-	-	-	1	-	-	-	-	1	1	-	-	-	-	-	-	-	-	-	-	-	-
00-179	04:04	3.270	3.843																								
00-208	01:04	3.100	28.87	6	-	-	-	3	1	-	1	-	-	-	-	-	-	-	-	-	-	-	-	-	-	-	-
00-237	08:51	2.920	29.32	10	-	-	1	1	2	-	-	-	-	-	-	-	-	-	-	-	-	-	-	-	-	-	-
00-259	19:44	2.770	22.45	5	-	-	2	1	-	-	1	-	-	-	3	-	-	-	-	-	-	-	-	-	-	-	-
00-284	01:25	2.610	24.23	4	-	-	-	-	1	1	-	-	-	-	1	-	-	-	-	-	-	-	-	-	-	-	-
00-310	04:17	2.430	26.11	5	-	-	1	-	1	-	3	-	-	-	1	-	-	-	-	-	-	-	-	-	-	-	-
00-340	13:32	2.220	30.38	7	-	1	-	-	1	-	1	-	-	-	4	-	-	-	-	-	-	-	-	-	-	-	-
01-014	16:49	1.930	39.13	9	-	2	3	-	-	-	2	-	-	-	4	-	-	-	1	-	-	-	-	-	-	-	-
01-039	10:03	1.770	24.71	2	-	-	-	2	1	1	1	-	-	-	-	-	-	1	1	-	-	-	-	-	-	-	-
01-054	10:21	1.670	15.01	8	2	-	-	1	1	-	2	-	-	-	1	-	-	-	1	-	-	-	-	-	-	-	-
01-080	01:19	1.520	25.62	8	2	-	1	1	1	-	1	-	1	2	-	-	-	-	-	-	1	-	-	-	-	-	-
01-100	19:10	1.430	20.74	10	-	-	-	1	1	-	2	-	-	-	-	-	1	-	2	-	-	-	-	-	-	-	-
01-120	16:27	1.370	19.88	16	-	-	1	3	-	-	3	-	-	-	1	-	-	-	1	1	-	-	1	-	1	-	-
01-141	01:45	1.340	20.38	31	-	2	3	2	1	-	2	-	1	-	1	-	3	-	2	-	1	-	-	-	-	-	-
01-165	00:33	1.360	23.95	38	1	-	-	4	-	-	-	-	1	1	1	-	1	-	2	-	-	1	-	1	2	1	1
01-189	15:48	1.440	24.63	13	-	-	-	2	-	-	1	-	-	2	2	-	-	-	-	-	-	-	-	1	-	-	1
01-206	16:29	1.520	17.02	7	-	-	-	-	-	-	-	-	2	-	1	-	-	-	1	-	-	-	-	-	-	-	-
01-232	07:47	1.670	25.63	4	-	-	-	1	-	-	-	-	-	-	1	-	-	-	-	-	-	-	-	-	-	-	-
01-256	00:16	1.820	23.68	5	-	-	-	3	-	-	1	1	-	-	-	-	-	-	1	-	-	-	-	-	-	-	-
1-274	15:41	1.950	18.64	4	-	-	-	-	-	-	-	-	-	-	1	-	-	-	-	-	-	-	-	-	-	-	-
01-306	23:07	2.180	32.30	2	1	-	-	1	1	-	-	-	-	-	1	-	-	-	-	-	-	-	-	-	-	-	-
01-336	22:47	2.390	29.98	3	-	-	-	1	-	-	-	-	-	-	1	-	-	-	-	-	-	-	-	-	-	-	-
01-354	03:39	2.510	17.20	1	-	-	-	-	-	-	-	-	-	-	-	-	-	-	-	-	-	-	-	-	-	-	-
02-016	23:24	2.700	27.82	5	-	-	1	-	-	-	-	-	-	-	1	-	-	-	1	-	-	-	-	-	-	-	-
02-036	13:27	2.820	19.58	2	-	-	1	-	-	-	-	-	-	-	-	-	-	-	-	-	-	-	-	-	-	-	-
02-083	00:56	3.120	46.47	1	-	-	-	-	1	-	2	-	2	-	3	-	-	-	-	-	-	-	-	-	-	-	-
02-085	02:26	3.130	2.062																								
02-113	23:19	3.300	28.87	-	1	1	-	-	-	2	-	-	-	-	-	-	-	-	2	*	-	-	-	*	-	-	-
02-147	16:16	3.490	33.70	-	1	3	-	-	1	3	2	-	-	-	-	-	-	-	-	*	-	-	-	*	-	-	-
02-175	09:59	3.640	27.73	-	1	2	-	-	-	1	2	-	-	-	1	-	-	-	1	*	-	-	-	*	-	-	-
02-200	10:24	3.760	25.01	-	2	1	-	-	-	1	-	-	-	-	3	-	-	-	-	*	-	-	-	*	-	-	-
02-225	16:31	3.890	25.25	-	-	2	2	-	2	1	-	-	-	-	3	-	-	-	1	*	-	-	-	*	-	-	-
02-253	13:08	4.020	27.85	-	2	1	-	-	1	3	1	-	-	-	1	-	-	-	-	*	-	-	-	*	-	-	-
02-277	21:53	4.120	24.36	-	2	1	-	-	-	2	-	-	-	-	1	-	-	-	-	*	-	-	-	*	-	-	-

02-305	19:50	4.240	27.91	-	-	-	-	-	1	-	3	-	-	1	-	-	-	-	-	*	-	-	-	*	-	-	-
02-334	08:07	4.350	28.51	-	-	22	3	-	-	2	2	-	-	-	2	-	-	-	-	*	-	-	-	*	-	-	-
03-154	03:33	4.930	184.8																								
03-183	07:57	5.000	29.18	-	3	7	-	-	-	1	1	-	-	-	1	-	-	-	-	*	-	-	1	*	-	-	-
03-195	08:29	5.030	12.02	-	7	121	26	-	-	2	-	-	-	-	1	-	-	-	-	*	-	-	-	*	-	-	-
3-203	06:00	5.050	7.896	-	-	2	-	-	1	-	-	-	-	-	-	-	-	-	-	*	-	-	-	*	-	-	-
03-234	17:39	5.110	31.48																								
03-256	20:30	5.150	22.11	-	4	31	9	-	-	1	2	-	-	-	-	-	-	-	-	*	-	-	-	*	-	-	-
03-284	21:58	5.200	28.06	-	1	15	5	-	2	1	-	-	-	-	-	-	-	-	1	*	-	-	-	*	-	-	-
03-315	14:30	5.250	30.68	-	5	95	18	-	-	3	3	-	-	-	-	-	-	-	-	*	-	-	-	*	-	-	-
03-337	14:42	5.280	22.00	-	4	111	22	-	-	5	3	-	-	-	-	-	-	-	-	*	-	-	-	*	-	-	-
03-360	07:06	5.300	22.68	-	-	124	22	-	-	1	2	-	-	-	1	-	-	-	-	*	-	-	-	*	-	-	-
04-025	18:39	5.330	31.48	-	2	28	6	-	-	1	-	-	-	-	1	-	-	-	-	*	-	-	-	*	-	-	-
04-074	22:15	5.370	49.15	-	2	46	9	-	-	3	1	-	-	-	2	-	-	-	-	*	-	-	-	*	-	-	-
04-088	19:10	5.380	13.87	-	2	93	11	-	1	-	1	-	-	1	-	-	-	-	-	*	-	-	-	*	-	-	-
04-135	12:32	5.400	46.72	-	1	13	2	-	-	-	4	-	-	1	1	-	-	-	-	*	-	-	-	*	-	-	-
04-156	15:14	5.410	21.11	-	2	162	50	-	-	3	2	-	-	-	-	-	-	1	-	*	-	-	-	*	-	-	-
04-166	00:14	5.410	9.375	-	3	886	184	-	-	-	-	-	-	-	-	-	-	-	-	*	-	-	-	*	-	-	-
04-168	08:16	5.410	2.334	-	11	1931	463	-	1	-	-	-	-	-	-	-	-	-	-	*	-	-	-	*	-	-	-
04-179	16:33	5.410	11.34	1	6	874	228	-	-	1	-	-	-	-	-	-	-	-	-	*	-	-	-	*	-	-	-
04-205	11:10	5.410	25.77	-	4	188	62	-	-	3	2	-	-	1	1	-	-	-	-	*	-	-	-	*	-	-	-
04-235	05:29	5.400	29.76	-	5	24	5	-	-	1	-	-	-	1	1	-	-	-	1	*	-	-	-	*	-	-	-
04-263	11:10	5.390	28.23	-	4	11	2	-	1	2	-	-	-	1	2	-	-	-	-	*	-	-	-	*	-	-	-
04-293	00:54	5.370	29.57	-	4	8	1	-	-	2	2	-	-	-	1	-	-	-	-	*	-	-	-	*	-	-	-
04-335	02:06	5.340	42.05	-	4	32	4	-	-	5	2	-	-	-	1	-	-	-	4	*	-	-	-	*	-	-	-
04-337	11:00	5.340	2.370																								
04-365	22:16	5.310	28.46	-	2	7	3	-	1	2	1	-	-	-	-	-	-	-	-	*	-	-	-	*	-	-	-
Impacts (counted)				-	-	4847	1153	-	28	54	60	2	7	12	57	0	5	2	23	0	2	1	2	0	3	1	2
Impacts (complete data)				228	92	2677	1128	29	28	54	60	2	7	12	57	0	5	2	23	0	2	1	2	0	3	1	2
All events(complete data)				43807	2109	2963	1144	593	28	54	60	3	7	12	57	0	5	2	23	0	2	1	2	0	3	1	2

Switch-on of the instrument is indicated by horizontal lines. The heliocentric distance R, the lengths of the time interval Δt (days) from the previous table entry, and the corresponding numbers of impacts are given for the 24 accumulators. The accumulators are arranged with increasing signal amplitude ranges (AR), with four event classes for each amplitude range (CLN = 0,1,2,3); e.g. AC31 means counter for AR = 1 and CLN = 3. The Δt in the first line (00-001) is the time interval counted from the last entry in Table 3 in Paper VII. The totals of counted impacts[a], of impacts with complete data, and of all events (noise plus impact events) for the entire period are given as well.

[a]:Entries for AC01, AC11 and AC02 are the number of impacts with complete data. Due to the noise contamination of these three categories the number of impacts cannot be determined from the accumulators. The method to separate dust impacts from noise events in these three categories has been given by Baguhl et al. (1993).

Table 3
Raw data: no., impact time, CLN, AR, SEC, IA, EA, CA, IT, ET, EIT, EIC, ICC, PA, PET, EVD, ICP, ECP, CCP, PCP, HV and evaluated data: R, LON, LAT, D_{Jup} (in jovian radii $R_{\mathrm{J}} = 71\,492$ km), rotation angle (ROT), instr. pointing (S_{LON}, S_{LAT}), impact speed (v, in km s^{-1}), speed error factor (VEF), mass (m, in grams) and mass error factor (MEF)

No.	IMP. DATE	CLN	AR	SEC	IA	EA	CA	IT	ET	EIT	EIC	IIC	PA	PET	EVD	ICP	ECP	CCP	PCP	HV	R	LON	LAT	D_{Jup}	ROT	S_{LON}	S_{LAT}	V	VEF	M	MEF
1697	00-014 15:31	3	3	131	20	25	9	6	6	6	0	1	44	0	1	0	0	0	1	3	4.10249	165.5	−36.0	16448.0	91	276	3	28.0	1.6	$5.9 \cdot 10^{-13}$	6.0
1699	00-017 10:35	0	2	51	10	5	0	9	15	0	1	0	44	31	1	0	0	0	1	3	4.09054	165.5	−36.2	16408.6	338	146	49	14.1	1.9	$1.1 \cdot 10^{-13}$	10.5
1700	00-021 12:16	0	2	139	9	14	0	7	7	6	0	0	36	0	1	0	0	0	1	3	4.07249	165.6	−36.5	16349.5	107	286	−8	43.7	1.6	$6.4 \cdot 10^{-15}$	6.0
1703	00-033 23:18	3	3	116	23	29	18	6	4	5	0	1	46	0	1	0	0	0	1	3	4.01748	166.0	−37.6	16171.7	88	271	5	38.7	1.6	$6.2 \cdot 10^{-13}$	6.0
1704	00-036 09:06	3	3	82	21	26	3	5	5	6	0	1	46	0	1	0	0	0	1	3	4.00621	166.0	−37.8	16135.6	44	235	34	43.7	1.6	$1.6 \cdot 10^{-13}$	6.0
1705	00-038 03:08	1	2	82	15	7	9	9	15	0	1	1	38	31	1	0	0	0	1	3	3.99829	166.1	−38.0	16110.4	44	235	34	14.1	1.9	$3.1 \cdot 10^{-13}$	10.5
1707	00-047 22:40	0	3	116	20	7	0	5	0	6	0	0	46	0	1	0	0	0	1	3	3.95368	166.3	−38.8	15969.5	110	284	−8	34.1	1.9	$2.5 \cdot 10^{-14}$	10.5
1709	00-056 07:20	3	2	167	9	14	1	7	7	6	0	1	35	0	1	0	0	0	1	3	3.91470	166.6	−39.6	15848.2	191	6	−33	43.7	1.6	$6.4 \cdot 10^{-15}$	6.0
1712	00-075 21:27	1	2	83	12	10	10	9	15	0	1	1	5	31	1	0	0	0	1	3	3.82095	167.2	−41.4	15563.3	112	274	−8	14.1	1.9	$3.5 \cdot 10^{-13}$	10.5
1713	00-079 06:35	3	3	62	20	25	6	5	5	6	0	1	44	0	1	0	0	0	1	3	3.80449	167.3	−41.8	15514.3	88	253	5	43.7	1.6	$1.1 \cdot 10^{-13}$	6.0
1727	00-134 11:13	3	3	48	20	25	5	7	7	6	0	1	43	0	1	0	0	0	1	3	3.52098	169.5	−47.5	14717.9	138	277	−23	21.0	1.6	$1.8 \cdot 10^{-12}$	6.0
1729	00-158 09:12	1	2	3	10	7	3	10	15	0	1	1	0	0	1	0	0	0	1	3	3.38877	170.8	−50.3	14377.9	90	238	4	10.4	1.9	$3.1 \cdot 10^{-13}$	10.5
1732	00-175 07:49	2	3	48	21	28	8	7	5	5	0	1	46	0	1	0	0	0	0	4	3.29256	171.9	−52.3	14143.1	165	309	−35	14.1	1.9	$1.5 \cdot 10^{-11}$	10.5
1733	00-180 23:19	0	2	74	8	1	0	7	15	0	1	0	0	0	1	0	0	0	1	3	3.25988	172.3	−53.1	14065.8	205	359	−32	34.1	1.9	$1.8 \cdot 10^{-15}$	10.5
1736	00-189 10:42	0	2	97	8	13	0	7	7	6	0	0	34	0	1	0	0	0	1	3	3.20994	172.9	−54.2	13950.1	243	36	−13	43.7	1.6	$4.7 \cdot 10^{-15}$	6.0
1738	00-203 17:47	1	2	34	12	7	10	9	11	15	1	1	36	14	1	0	0	0	1	3	3.12468	174.1	−56.1	13759.3	163	313	−35	14.1	1.9	$2.1 \cdot 10^{-13}$	10.5
1741	00-205 11:15	0	2	37	10	6	0	9	15	0	1	0	0	0	1	0	0	0	1	3	3.11407	174.2	−56.4	13736.2	170	322	−37	14.1	1.9	$1.3 \cdot 10^{-13}$	10.5
1742	00-206 02:02	3	2	104	9	13	9	7	7	6	0	1	35	0	1	0	0	0	1	3	3.11028	174.3	−56.4	13727.9	264	57	0	43.7	1.6	$5.4 \cdot 10^{-15}$	6.0
1745	00-212 14:52	1	2	198	11	7	6	8	15	15	1	1	35	31	1	0	0	0	1	3	3.07060	174.9	−57.4	13642.8	40	209	36	21.4	1.9	$3.8 \cdot 10^{-14}$	10.5
1746	00-213 08:54	1	2	215	10	7	9	9	15	0	1	1	37	31	1	0	0	0	1	3	3.06599	175.0	−57.5	13633.0	66	233	20	14.1	1.9	$1.5 \cdot 10^{-13}$	10.5
1755	00-235 05:07	0	2	22	8	13	0	7	7	7	0	0	35	0	1	0	0	0	1	3	2.92938	177.5	−60.7	13354.7	169	332	−36	43.7	1.6	$4.7 \cdot 10^{-15}$	6.0
1758	00-238 22:54	3	2	80	9	14	12	7	7	6	0	1	36	0	1	0	0	0	1	3	2.90552	178.0	−61.3	13308.4	253	61	−6	43.7	1.6	$6.4 \cdot 10^{-15}$	6.0
1762	00-241 10:03	0	2	243	11	20	0	7	6	7	0	0	38	0	1	0	0	0	1	3	2.88953	178.4	−61.7	13277.7	125	290	−18	34.1	1.9	$4.4 \cdot 10^{-14}$	10.5
1765	00-244 10:11	3	3	179	22	27	18	7	6	5	0	1	47	0	1	0	0	0	1	4	2.87028	178.8	−62.2	13241.2	35	216	38	22.7	1.6	$2.4 \cdot 10^{-12}$	6.0
1766	00-251 21:17	3	3	192	20	26	11	8	6	5	0	1	46	0	1	0	0	0	1	4	2.82179	180.0	−63.4	13151.2	59	242	24	19.5	1.6	$2.8 \cdot 10^{-12}$	6.0
1767	00-253 16:00	3	3	207	19	25	4	6	6	6	0	1	44	0	1	0	0	0	1	4	2.81040	180.3	−63.7	13130.5	83	263	9	28.0	1.6	$4.4 \cdot 10^{-13}$	6.0
1770	00-263 00:00	3	3	228	22	27	14	6	5	5	0	1	47	0	0	0	0	0	1	4	2.74895	182.1	−65.3	13021.3	117	293	−12	34.6	1.6	$5.9 \cdot 10^{-13}$	6.0
1772	00-273 09:50	1	2	216	9	8	11	10	15	0	1	1	36	31	1	0	0	0	1	4	2.68005	184.5	−67.1	12904.3	106	291	−5	10.4	1.9	$3.2 \cdot 10^{-13}$	10.5
1774	00-278 02:46	2	2	214	11	19	5	8	6	7	0	1	36	0	1	0	0	0	1	4	2.64906	185.7	−67.9	12853.5	104	292	−4	21.4	1.9	$1.7 \cdot 10^{-13}$	10.5
1777	00-287 13:55	3	2	103	8	13	1	7	8	6	0	1	0	0	1	0	0	0	1	4	2.58485	188.6	−69.6	12752.0	311	135	28	35.4	1.6	$1.1 \cdot 10^{-14}$	6.0
1780	00-295 18:41	3	3	171	20	24	8	6	6	6	0	1	43	0	1	0	0	0	1	4	2.52855	191.6	−71.1	12666.9	50	259	27	28.0	1.6	$5.1 \cdot 10^{-13}$	6.0
1781	00-296 13:33	3	2	178	14	21	7	7	7	6	0	1	39	0	1	0	0	0	1	4	2.52341	191.9	−71.2	12659.4	59	268	22	34.1	1.9	$8.3 \cdot 10^{-14}$	10.5
1782	00-300 06:46	3	2	176	13	21	1	8	5	7	0	1	41	0	1	0	0	0	1	4	2.49763	193.6	−71.9	12621.9	59	272	22	21.4	1.9	$3.6 \cdot 10^{-13}$	10.5
1783	00-303 05:05	1	2	142	9	2	1	9	15	0	1	1	46	31	1	0	0	0	1	4	2.47781	194.9	−72.5	12593.6	12	224	40	14.1	1.9	$5.8 \cdot 10^{-14}$	10.5
1788	00-312 00:53	3	2	244	8	12	7	7	7	6	0	1	0	0	1	0	0	0	1	4	2.41629	199.8	−74.1	12508.8	157	9	−26	43.7	1.6	$4.0 \cdot 10^{-15}$	6.0
1789	00-313 00:18	3	3	141	19	22	5	7	6	6	0	1	42	0	1	0	0	0	1	4	2.40933	200.5	−74.3	12499.5	11	230	39	22.7	1.6	$5.8 \cdot 10^{-13}$	6.0
1791	00-315 18:22	3	3	163	22	28	10	6	5	5	0	1	47	0	1	0	0	0	1	4	2.39016	202.3	−74.7	12474.1	43	269	29	34.6	1.6	$7.0 \cdot 10^{-13}$	6.0
1795	00-322 19:23	3	3	205	23	29	8	7	4	6	0	1	47	0	1	0	0	0	1	4	2.34119	207.6	−75.9	12411.3	101	326	−1	31.4	1.8	$1.3 \cdot 10^{-12}$	9.5
1798	00-332 21:26	1	2	129	10	6	14	9	11	15	1	1	0	0	1	0	0	0	1	4	2.26997	217.5	−77.5	12325.0	353	227	38	14.1	1.9	$1.3 \cdot 10^{-13}$	10.5
1800	00-336 14:15	3	3	139	22	29	7	9	4	6	0	1	47	0	1	0	0	0	1	4	2.24439	221.8	−78.0	12295.5	7	248	38	7.8	1.9	$9.1 \cdot 10^{-11}$	10.5
1804	00-345 05:03	3	3	158	20	26	12	9	6	6	0	1	1	0	1	0	0	0	1	4	2.18340	233.8	−78.8	12228.1	32	288	32	16.9	1.8	$4.9 \cdot 10^{-12}$	8.4
1810	00-351 19:21	3	3	154	19	23	9	7	7	6	0	1	42	0	1	0	0	0	1	4	2.13650	244.4	−79.1	12179.3	24	287	35	21.0	1.6	$9.6 \cdot 10^{-13}$	6.0
1811	00-353 03:29	3	3	199	19	24	5	6	6	6	0	1	44	0	1	0	0	0	1	4	2.12676	246.7	−79.1	12169.4	87	350	6	28.0	1.6	$3.8 \cdot 10^{-13}$	6.0
1813	00-354 00:26	3	3	149	23	29	18	6	5	6	0	1	47	0	1	0	0	0	1	4	2.12057	248.2	−79.1	12163.2	17	281	37	34.6	1.6	$9.8 \cdot 10^{-13}$	6.0
1815	00-360 23:05	3	2	162	15	22	17	8	8	6	0	1	40	0	1	0	0	0	1	4	2.07193	260.0	−78.9	12116.1	33	310	33	21.4	1.9	$5.4 \cdot 10^{-13}$	10.5

1816	01-001 22:45	3	4	121	25	49	12	7	4	5	0	1	47	0	1	0	0	0	1	4	2.02958	269.9	−78.2	12077.3	334	244	36	14.1	1.9	$6.5 \cdot 10^{-11}$	10.5
1817	01-001 01:02	3	2	113	14	22	1	8	7	6	0	1	41	0	1	0	0	0	1	4	2.02870	270.1	−78.2	12076.5	323	232	32	21.4	1.9	$5.0 \cdot 10^{-13}$	10.5
1822	01-016 13:27	2	4	160	27	49	17	7	5	5	0	1	47	0	1	0	0	0	1	4	1.92015	291.2	−75.1	11986.1	28	329	38	14.1	1.9	$9.0 \cdot 10^{-11}$	10.5
1823	01-016 19:03	1	2	86	14	14	12	11	15	15	1	1	10	31	1	0	0	0	1	4	1.91842	291.5	−75.0	11984.8	284	212	12	7.8	1.9	$4.1 \cdot 10^{-12}$	10.5
1825	01-024 14:45	3	4	143	26	49	17	6	5	5	0	1	47	0	1	0	0	0	1	4	1.86494	299.2	−72.7	11945.1	4	307	45	21.4	1.9	$1.7 \cdot 10^{-11}$	10.5
1826	01-024 20:26	3	2	109	14	23	1	8	6	6	0	1	42	0	1	0	0	0	1	4	1.86322	299.4	−72.7	11943.9	316	247	32	21.4	1.9	$5.8 \cdot 10^{-13}$	10.5
1827	01-031 20:19	0	2	135	8	12	0	8	8	7	0	0	0	0	1	0	0	0	1	4	1.81560	305.0	−70.3	11911.1	354	299	47	28.0	1.6	$2.1 \cdot 10^{-14}$	6.0
1828	01-035 13:12	0	2	152	8	8	0	9	15	15	1	0	46	30	1	0	0	0	1	4	1.79041	307.6	−68.9	11894.8	18	338	46	14.1	1.9	$1.3 \cdot 10^{-13}$	10.5
1829	01-037 12:32	2	2	157	12	20	1	7	6	6	0	1	39	0	1	0	0	0	1	4	1.77708	308.9	−68.1	11886.4	26	351	44	34.1	1.9	$5.2 \cdot 10^{-14}$	10.5
1832	01-042 03:42	1	2	132	10	12	1	11	3	0	1	1	63	5	1	0	0	0	1	4	1.74656	311.6	−66.2	11867.8	352	305	51	23.4	2.9	$5.3 \cdot 10^{-14}$	42.3
1837	01-044 08:12	3	4	130	26	49	17	6	5	5	0	1	47	0	1	0	0	0	1	4	1.73269	312.7	−65.3	11859.7	350	304	51	21.4	1.9	$1.7 \cdot 10^{-11}$	10.5
1839	01-045 03:11	3	2	184	10	14	7	7	8	6	0	1	35	0	1	0	0	0	1	4	1.72701	313.2	−64.9	11856.5	67	37	20	35.4	1.6	$1.8 \cdot 10^{-14}$	6.0
1840	01-045 13:32	3	3	122	23	29	8	6	5	6	0	1	47	0	1	0	0	0	1	4	1.72458	313.4	−64.8	11855.1	340	289	48	34.6	1.6	$9.8 \cdot 10^{-13}$	6.0
1841	01-046 00:41	0	2	71	9	14	0	7	7	7	0	0	37	0	1	0	0	0	1	4	1.72134	313.6	−64.5	11853.2	268	225	2	43.7	1.6	$6.4 \cdot 10^{-15}$	6.0
1844	01-047 03:46	3	2	143	13	21	1	7	4	6	0	1	40	0	1	0	0	0	1	4	1.71409	314.2	−64.0	11849.1	10	337	52	34.1	1.9	$7.1 \cdot 10^{-14}$	10.5
1847	01-057 01:38	0	2	185	11	20	0	7	6	6	0	0	40	0	1	0	0	0	1	4	1.65193	318.4	−59.4	11816.1	75	52	15	34.1	1.9	$4.4 \cdot 10^{-14}$	10.5
1848	01-060 07:55	1	5	91	54	24	27	14	1	15	1	1	23	6	1	0	0	0	1	4	1.63213	319.7	−57.8	11806.3	304	258	30	2.0	1.9	$5.0 \cdot 10^{-08}$	10.5
1849	01-061 04:02	1	2	106	9	12	9	8	15	15	1	1	1	30	1	0	0	0	1	4	1.62686	320.0	−57.4	11803.7	326	278	46	7.0	2.9	$1.9 \cdot 10^{-12}$	46.7
1854	01-068 17:45	2	3	160	22	29	5	8	5	6	0	1	47	0	1	0	0	0	1	4	1.58288	322.4	−53.4	11783.3	48	43	37	10.4	1.9	$4.2 \cdot 10^{-11}$	10.5
1855	01-069 20:58	1	3	84	21	22	8	11	11	13	1	1	47	26	1	0	0	0	1	4	1.57647	322.8	−52.8	11780.5	302	261	29	2.5	1.9	$1.0 \cdot 10^{-09}$	10.5
1858	01-072 07:30	2	3	62	23	30	12	8	5	5	0	1	47	0	1	0	0	0	1	4	1.56244	323.5	−51.4	11774.3	273	245	5	10.4	1.9	$5.8 \cdot 10^{-11}$	10.5
1861	01-074 20:31	3	2	133	10	14	7	7	7	6	0	1	36	0	1	0	0	0	1	4	1.54870	324.2	−50.0	11768.5	15	10	60	43.7	1.6	$7.5 \cdot 10^{-15}$	6.0
1865	01-082 01:30	3	4	146	26	49	17	6	6	5	0	1	47	0	1	0	0	0	1	4	1.51057	326.1	−45.7	11752.8	41	49	44	21.4	1.9	$1.7 \cdot 10^{-11}$	10.5
1867	01-084 18:19	3	2	200	8	20	3	9	12	15	0	1	20	1	1	0	0	0	1	4	1.49683	326.7	−44.0	11747.3	120	94	−22	14.1	1.9	$6.5 \cdot 10^{-13}$	10.5
1869	01-090 18:12	3	2	86	9	11	1	10	9	15	0	1	17	1	1	0	0	0	1	4	1.46840	328.1	−40.2	11736.1	326	284	51	18.0	1.6	$1.1 \cdot 10^{-13}$	6.0
1870	01-090 21:34	0	2	79	8	13	0	8	7	7	0	0	36	0	1	0	0	0	1	4	1.46784	328.1	−40.1	11735.9	316	277	43	34.6	1.6	$1.2 \cdot 10^{-14}$	6.0
1871	01-091 20:14	1	2	111	10	10	2	8	15	15	1	1	42	30	1	0	0	0	1	4	1.46388	328.3	−39.5	11734.3	2	354	69	21.4	1.9	$5.6 \cdot 10^{-14}$	10.5
1873	01-094 23:08	1	4	110	27	29	27	8	5	15	1	1	13	4	1	0	0	0	1	4	1.45017	329.0	−37.4	11729.0	4	2	70	24.1	2.0	$6.1 \cdot 10^{-12}$	11.5
1874	01-096 06:02	3	4	69	25	31	28	7	5	5	0	1	47	0	1	0	0	0	1	4	1.44434	329.3	−36.5	11726.7	308	272	37	28.1	1.6	$3.3 \cdot 10^{-12}$	6.0
1882	01-101 23:02	3	5	65	53	49	21	14	5	5	0	1	63	0	1	0	0	0	1	4	1.42189	330.4	−32.7	11717.7	308	274	37	2.0	1.9	$2.0 \cdot 10^{-07}$	10.5
1885	01-105 21:30	0	2	160	8	13	0	7	7	6	0	0	0	0	1	0	0	0	1	4	1.40735	331.1	−29.9	11711.6	86	89	5	43.7	1.6	$4.7 \cdot 10^{-15}$	6.0
1886	01-106 03:23	3	2	74	14	21	8	8	9	6	0	1	40	0	1	0	0	0	1	4	1.40649	331.1	−29.7	11711.2	326	284	53	21.4	1.9	$4.2 \cdot 10^{-13}$	10.5
1888	01-107 14:27	3	3	154	22	30	4	10	4	5	0	1	47	0	1	0	0	0	1	4	1.40180	331.4	−28.7	11709.2	79	87	12	5.0	1.9	$4.4 \cdot 10^{-10}$	10.5
1890	01-110 15:07	0	2	56	9	19	0	8	5	7	0	0	37	0	1	0	0	0	1	4	1.39173	332.0	−26.4	11704.6	305	274	34	21.4	1.9	$1.2 \cdot 10^{-13}$	10.5
1892	01-113 16:25	3	2	77	11	20	2	7	6	6	0	1	38	0	1	0	0	0	1	4	1.38281	332.5	−24.2	11700.3	337	293	65	34.1	1.9	$4.4 \cdot 10^{-14}$	10.5
1894	01-114 07:32	0	2	151	10	19	0	7	5	7	0	0	37	0	1	0	0	0	1	4	1.38105	332.6	−23.8	11699.4	82	92	9	34.1	1.9	$2.9 \cdot 10^{-14}$	10.5
1899	01-115 13:55	1	6	52	58	28	31	6	0	1	1	1	29	1	1	0	0	0	1	4	1.37763	332.8	−22.8	11697.6	304	274	34	21.4	1.9	$8.3 \cdot 10^{-11}$	10.5
1901	01-116 19:28	3	2	63	10	19	3	6	6	6	0	1	37	0	1	0	0	0	1	4	1.37434	333.0	−21.9	11695.8	320	280	50	43.5	1.9	$1.1 \cdot 10^{-14}$	10.5
1903	01-117 04:39	3	4	43	24	28	10	6	5	6	0	1	47	0	1	0	0	0	1	4	1.37338	333.1	−21.6	11695.3	292	271	23	34.6	1.6	$9.6 \cdot 10^{-13}$	6.0
1910	01-121 12:03	1	2	61	8	13	1	7	13	15	1	1	26	18	1	0	0	0	1	4	1.36313	333.8	−18.3	11689.0	321	280	51	16.2	1.7	$2.0 \cdot 10^{-13}$	7.4
1912	01-122 09:11	1	4	90	31	30	18	7	7	15	1	1	47	2	1	0	0	0	1	4	1.36128	333.9	−17.7	11687.7	3	25	82	14.1	1.9	$9.3 \cdot 10^{-11}$	10.5
1915	01-123 16:25	0	2	87	9	14	0	7	7	7	0	0	37	0	1	0	0	0	1	4	1.35877	334.1	−16.7	11685.9	360	2	83	43.7	1.6	$6.4 \cdot 10^{-15}$	6.0
1917	01-123 23:35	3	3	47	18	12	7	13	5	15	0	1	13	1	1	0	0	0	1	4	1.35829	334.2	−16.5	11685.5	304	275	34	2.0	1.9	$3.8 \cdot 10^{-10}$	10.5
1918	01-125 00:17	1	3	88	22	22	19	12	11	13	1	1	10	27	1	0	0	0	1	4	1.35618	334.4	−15.6	11683.9	2	24	84	2.0	1.9	$3.2 \cdot 10^{-09}$	10.5
1919	01-125 15:18	3	2	117	9	26	1	12	9	15	0	1	62	14	1	0	0	0	1	4	1.35506	334.5	−15.2	11683.0	43	90	47	5.0	1.9	$3.5 \cdot 10^{-11}$	10.5
1922	01-126 21:42	3	4	102	28	49	19	5	5	5	0	1	47	0	1	0	0	0	1	4	1.35293	334.6	−14.2	11681.1	23	84	66	34.1	1.9	$4.5 \cdot 10^{-12}$	10.5
1925	01-127 23:24	1	4	139	29	9	11	8	0	5	0	1	1	0	1	0	0	0	1	4	1.35133	334.8	−13.4	11679.6	76	98	15	10.4	1.9	$7.1 \cdot 10^{-12}$	10.5
1928	01-128 15:42	0	2	163	13	10	0	9	15	15	1	0	46	30	1	0	0	0	1	4	1.35019	334.9	−12.8	11678.5	110	104	−18	14.1	1.9	$4.1 \cdot 10^{-13}$	10.5
1936	01-133 10:45	1	4	254	24	6	21	13	5	10	1	1	62	20	1	0	0	0	1	4	1.34426	335.7	−9.1	11671.3	242	269	−26	2.0	1.9	$4.5 \cdot 10^{-10}$	10.5
1938	01-136 17:31	3	2	64	11	9	1	7	1	10	0	1	31	1	1	0	0	0	1	4	1.34146	336.2	−6.6	11666.1	337	278	67	34.1	1.9	$1.1 \cdot 10^{-14}$	10.5
1939	01-136 20:56	3	4	63	27	49	27	6	5	5	0	1	47	0	1	0	0	0	1	4	1.34137	336.2	−6.5	11665.9	335	278	65	21.4	1.9	$2.0 \cdot 10^{-11}$	10.5
1954	01-139 22:14	1	5	79	53	49	30	13	15	0	1	1	27	3	1	0	1	0	1	3	1.33971	336.7	−4.0	11660.8	359	205	88	2.0	1.9	$2.0 \cdot 10^{-07}$	10.5

Table 3 (*continued*)

No.	IMP. DATE	CLN	AR	SEC	IA	EA	CA	IT	ET	EIT	EIC	IIC	PA	PET	EVD	ICP	ECP	CCP	PCP	HV	R	LON	LAT	D_{Jup}	ROT	S_{LON}	S_{LAT}	V	VEF	M	MEF
1956	01-141 08:59	3	4	54	27	29	13	6	6	5	0	1	47	0	1	0	1	0	1	3	1.33928	336.9	−2.9	11658.5	325	276	55	28.0	1.6	$3.6 \cdot 10^{-12}$	6.0
1958	01-141 20:05	0	2	139	9	15	0	7	0	6	0	0	37	0	1	0	1	0	1	3	1.33917	337.0	−2.5	11657.6	85	106	5	34.1	1.9	$2.0 \cdot 10^{-14}$	10.5
1967	01-144 14:07	2	6	82	57	51	31	6	14	4	0	1	63	0	1	0	1	0	1	3	1.33902	337.4	−0.3	11652.9	6	140	82	21.4	1.9	$2.7 \cdot 10^{-10}$	10.5
1968	01-145 10:14	2	3	85	18	24	1	14	12	13	0	1	27	0	1	0	1	0	1	3	1.33913	337.5	0.3	11651.3	11	129	78	2.5	1.6	$6.6 \cdot 10^{-10}$	6.0
1969	01-145 11:47	1	6	27	58	29	30	6	3	4	1	1	31	0	1	0	1	0	1	3	1.33913	337.5	0.3	11651.3	289	278	19	21.4	1.9	$9.9 \cdot 10^{-11}$	10.5
1973	01-147 12:15	1	6	47	57	10	31	9	0	1	1	1	29	1	1	0	1	0	1	3	1.33972	337.8	2.0	11647.5	319	275	48	7.8	1.9	$1.1 \cdot 10^{-10}$	10.5
1976	01-148 05:21	3	4	56	30	31	25	10	11	6	0	1	23	0	1	0	1	0	1	3	1.33997	337.9	2.5	11646.3	331	271	61	5.0	1.9	$1.7 \cdot 10^{-09}$	10.5
1982	01-149 22:17	0	2	175	11	19	0	8	7	6	0	0	38	0	1	0	1	0	1	3	1.34090	338.2	3.9	11643.0	140	109	−49	21.4	1.9	$1.7 \cdot 10^{-13}$	10.5
1986	01-151 15:42	1	4	86	24	10	4	11	0	7	0	1	19	4	1	0	1	0	1	3	1.34213	338.5	5.3	11639.7	15	137	72	2.5	1.9	$3.6 \cdot 10^{-10}$	10.5
1988	01-152 02:35	1	3	32	18	21	9	12	15	0	1	1	18	30	1	0	1	0	1	3	1.34243	338.5	5.6	11638.9	299	278	29	2.5	1.6	$4.1 \cdot 10^{-10}$	6.0
1995	01-155 05:47	0	2	140	11	20	0	7	7	6	0	0	39	0	1	0	1	0	1	3	1.34549	339.0	8.0	11632.7	92	113	−2	34.1	1.9	$4.4 \cdot 10^{-14}$	10.5
1997	01-155 21:45	0	2	74	13	7	0	14	2	12	0	0	26	1	1	0	1	0	1	3	1.34636	339.1	8.6	11631.2	360	199	78	2.0	1.9	$1.2 \cdot 10^{-10}$	10.5
2004	01-160 11:22	3	6	80	56	30	30	12	3	4	0	1	63	0	1	0	1	0	1	3	1.35275	339.8	12.1	11621.6	10	166	72	2.0	1.9	$1.8 \cdot 10^{-07}$	10.5
2005	01-160 14:10	2	5	96	49	49	23	15	6	5	0	1	47	0	1	0	1	0	1	3	1.35296	339.8	12.2	11621.3	33	134	54	11.8	11.8	$3.4 \cdot 10^{-10}$	5858.3
2008	01-163 19:56	3	3	93	20	27	7	4	4	7	0	1	31	0	1	0	1	0	1	3	1.35881	340.3	14.7	11614.0	30	141	56	43.5	1.9	$1.6 \cdot 10^{-13}$	10.5
2013	01-167 01:58	2	3	91	19	24	9	6	6	5	0	1	42	0	1	0	1	0	1	3	1.36564	340.8	17.2	11606.4	28	148	56	28.0	1.6	$3.8 \cdot 10^{-13}$	6.0
2014	01-167 04:04	3	6	60	57	53	28	10	5	4	0	1	29	0	1	0	1	0	1	3	1.36593	340.9	17.3	11606.1	344	242	64	5.0	1.9	$2.8 \cdot 10^{-08}$	10.5
2015	01-168 01:06	3	2	127	14	22	3	9	9	5	0	1	36	0	1	0	1	0	1	3	1.36794	341.0	18.0	11604.0	79	122	10	14.1	1.9	$2.3 \cdot 10^{-12}$	10.5
2018	01-175 04:41	2	3	52	22	28	6	9	5	5	0	1	47	0	1	0	1	0	1	3	1.38686	342.2	23.3	11585.9	335	253	53	20.9	2.4	$4.1 \cdot 10^{-12}$	23.4
2020	01-177 22:31	3	3	144	19	23	3	6	6	5	0	1	42	0	1	0	1	0	1	3	1.39532	342.6	25.3	11578.5	105	118	−14	28.0	1.6	$3.3 \cdot 10^{-13}$	6.0
2021	01-177 22:42	0	2	38	8	19	0	13	7	7	0	0	27	2	1	0	1	0	1	3	1.39532	342.6	25.3	11578.5	316	271	38	2.5	1.9	$9.3 \cdot 10^{-11}$	10.5
2023	01-178 11:49	3	3	60	22	28	1	6	4	6	0	1	47	0	1	0	1	0	1	3	1.39693	342.7	25.6	11577.1	347	235	57	38.7	1.6	$4.4 \cdot 10^{-13}$	6.0
2025	01-181 09:45	0	2	196	9	14	0	7	7	6	0	0	4	31	1	0	1	0	1	3	1.40699	343.3	27.8	11568.7	178	36	−66	43.7	1.6	$6.4 \cdot 10^{-15}$	6.0
2031	01-191 02:00	1	3	86	19	19	9	8	6	0	1	1	44	7	1	0	1	0	1	3	1.44390	345.0	34.5	11539.7	25	183	42	10.4	1.9	$4.0 \cdot 10^{-12}$	10.5
2033	01-191 14:23	3	4	74	27	30	17	8	8	5	0	1	47	0	1	0	1	0	1	3	1.44600	345.1	34.8	11538.1	8	206	47	16.6	1.6	$3.2 \cdot 10^{-11}$	6.0
2037	01-197 19:26	1	3	96	19	19	12	12	7	0	1	1	37	8	1	0	1	0	1	3	1.47366	346.4	38.9	11517.6	40	176	30	2.0	1.9	$9.4 \cdot 10^{-10}$	10.5
2038	01-198 09:47	3	3	47	20	25	4	6	5	5	0	1	45	0	1	0	1	0	1	3	1.47656	346.5	39.3	11515.5	331	259	34	34.6	1.6	$3.0 \cdot 10^{-13}$	6.0
2042	01-212 12:09	3	3	48	23	29	4	7	5	5	0	1	47	0	1	0	1	0	1	3	1.54812	349.7	47.9	11464.5	335	264	25	28.1	1.6	$1.9 \cdot 10^{-12}$	6.0
2043	01-212 21:22	0	2	178	14	11	0	7	15	0	1	0	41	30	1	0	1	0	1	3	1.55016	349.8	48.2	11463.0	158	84	−34	34.1	1.9	$2.4 \cdot 10^{-14}$	10.5
2048	01-232 14:31	0	2	176	10	6	0	7	15	0	1	0	3	31	1	0	1	0	1	3	1.66517	355.8	58.6	11382.3	168	100	−23	34.1	1.9	$5.4 \cdot 10^{-15}$	10.5
2049	01-232 15:00	3	2	102	9	14	9	7	7	6	0	1	3	31	1	0	1	0	1	3	1.66595	355.8	58.6	11381.7	64	204	3	43.7	1.6	$6.4 \cdot 10^{-15}$	6.0
2050	01-235 12:55	3	4	24	30	49	7	7	6	5	0	1	47	0	1	0	1	0	1	3	1.68395	356.9	60.0	11369.0	318	316	8	14.1	1.9	$1.4 \cdot 10^{-10}$	10.5
2051	01-236 07:48	0	2	164	10	19	0	7	5	6	0	0	38	0	1	0	1	0	1	3	1.68868	357.2	60.4	11365.6	156	121	−20	34.1	1.9	$2.9 \cdot 10^{-14}$	10.5
2052	01-236 19:25	0	3	133	19	7	0	8	15	0	1	0	46	31	1	0	1	0	1	3	1.69185	357.4	60.6	11363.4	113	166	−10	10.4	1.9	$9.0 \cdot 10^{-13}$	10.5
2053	01-237 19:46	0	2	144	13	21	0	9	9	6	0	0	41	0	1	0	1	0	1	3	1.69820	357.8	61.1	11358.9	129	152	−15	14.1	1.9	$1.7 \cdot 10^{-12}$	10.5
2060	01-268 07:20	3	3	143	22	27	18	5	5	5	0	1	46	0	1	0	1	0	1	3	1.90205	16.0	72.9	11209.3	164	180	−18	43.7	1.6	$2.2 \cdot 10^{-13}$	6.0
2064	01-292 16:50	1	2	78	12	10	7	8	15	15	1	1	39	31	1	0	0	0	1	4	2.07289	45.3	78.3	11073.8	76	296	0	21.4	1.9	$7.6 \cdot 10^{-14}$	10.5
2066	01-302 11:48	3	3	149	19	24	20	6	6	6	0	1	43	0	1	0	0	0	1	4	2.14188	61.0	79.1	11015.8	174	205	−21	28.0	1.6	$3.8 \cdot 10^{-13}$	6.0
2067	01-303 10:34	0	2	165	9	14	0	8	8	7	0	0	36	0	1	0	0	0	1	4	2.14896	62.7	79.1	11009.7	196	182	−21	28.0	1.6	$3.3 \cdot 10^{-14}$	6.0
2071	01-311 15:36	3	3	166	22	28	28	5	4	6	0	1	47	0	1	0	0	0	1	4	2.20735	75.9	79.0	10958.7	194	189	−21	48.9	1.6	$1.7 \cdot 10^{-13}$	6.0
2072	01-325 04:24	0	2	102	10	20	0	8	5	6	0	0	38	0	1	0	0	0	1	4	2.30260	94.2	77.8	10872.0	98	296	−6	21.4	1.9	$1.9 \cdot 10^{-13}$	10.5
2077	01-357 07:41	3	4	146	24	31	26	9	5	5	0	1	47	0	1	0	0	0	1	4	2.52600	119.1	72.8	10649.3	139	266	−12	7.8	1.9	$1.6 \cdot 10^{-10}$	10.5
2082	02-016 15:01	3	3	165	19	23	2	5	6	7	0	1	42	0	1	0	0	0	1	4	2.69090	128.1	68.6	10465.1	135	262	−8	35.4	1.6	$1.5 \cdot 10^{-13}$	6.0
2087	02-046 00:40	1	3	1	19	20	13	9	5	0	1	1	37	4	1	0	0	0	1	4	2.88308	134.5	63.7	10226.0	121	164	−8	7.8	1.9	$1.1 \cdot 10^{-11}$	10.5
2089	02-050 23:20	3	2	214	13	22	7	8	7	6	0	1	41	0	1	0	0	0	1	4	2.91423	135.3	63.0	10184.5	54	228	1	21.4	1.9	$4.2 \cdot 10^{-13}$	10.5
2090	02-056 11:49	1	3	170	20	15	8	12	15	0	1	1	1	31	1	0	0	0	1	4	2.94911	136.1	62.1	10137.1	341	298	7	2.0	1.9	$1.0 \cdot 10^{-09}$	10.5
2091	02-058 23:42	3	3	253	21	27	12	6	6	6	0	1	46	0	1	0	0	0	1	4	2.96487	136.5	61.7	10115.3	98	182	−6	28.0	1.6	$9.8 \cdot 10^{-13}$	6.0
2092	02-066 12:39	1	2	9	14	6	1	9	15	0	1	1	43	31	1	0	0	0	0	5	3.01259	137.5	60.6	10048.1	107	174	−8	14.1	1.9	$2.4 \cdot 10^{-13}$	10.5

2093	02-080 00:20	3	3	249	19	22	11	6	6	6	0	1	41	0	1	0	0	0	1	4	3.09573	139.0	58.7	9926.2	71	211	2	28.0	1.6	$2.8 \cdot 10^{-13}$	6.0
2094	02-080 02:49	3	2	17	14	22	1	7	6	6	0	1	41	0	1	0	0	0	1	4	3.09573	139.0	58.7	9926.2	105	180	−9	34.1	1.9	$9.7 \cdot 10^{-14}$	10.5
2095	02-083 00:56	3	3	246	20	25	4	7	7	6	0	1	44	0	1	0	0	0	1	4	3.11397	139.3	58.3	9898.6	68	215	4	21.0	1.6	$1.8 \cdot 10^{-12}$	6.0
2096	02-108 13:31	3	4	219	25	49	14	6	4	5	0	1	47	0	1	0	0	0	1	4	3.26557	141.6	54.9	9656.5	11	277	28	21.4	1.9	$1.4 \cdot 10^{-11}$	10.5
2097	02-109 20:16	3	4	5	24	30	17	6	5	5	0	1	47	0	1	0	0	0	1	4	3.27284	141.7	54.7	9644.3	71	219	6	34.6	1.6	$1.3 \cdot 10^{-12}$	6.0
2099	02-113 08:08	2	2	77	9	14	0	7	8	6	0	0	36	0	1	0	0	0	1	4	3.29312	141.9	54.3	9609.9	170	124	−38	35.4	1.6	$1.6 \cdot 10^{-14}$	6.0
2100	02-113 19:08	2	2	77	9	14	0	8	8	6	0	0	35	0	1	0	0	0	1	4	3.29601	142.0	54.2	9605.0	170	124	−38	28.0	1.6	$3.3 \cdot 10^{-14}$	6.0
2105	02-130 02:20	3	2	45	14	21	4	7	7	7	0	1	39	0	1	0	0	0	1	4	3.38858	143.1	52.2	9442.2	117	188	−20	34.1	1.9	$8.3 \cdot 10^{-14}$	10.5
2106	02-133 04:46	1	2	212	8	9	0	7	15	0	1	0	13	31	1	0	0	0	1	4	3.40609	143.3	51.8	9410.4	350	310	35	34.1	1.9	$6.8 \cdot 10^{-15}$	10.5
2107	02-141 00:41	2	2	28	11	13	4	7	15	0	1	1	49	31	1	0	0	0	1	4	3.44982	143.8	50.9	9329.2	88	215	−1	8.9	4.3	$1.5 \cdot 10^{-12}$	179.4
2108	02-143 18:32	3	2	55	13	20	7	8	7	7	0	1	39	0	1	0	0	0	1	4	3.46495	143.9	50.6	9300.5	123	189	−25	21.4	1.9	$3.1 \cdot 10^{-13}$	10.5
2109	02-144 00:57	2	2	90	12	8	1	8	15	0	1	1	41	31	1	0	0	0	1	4	3.46632	143.9	50.6	9297.9	173	132	−47	21.4	1.9	$5.4 \cdot 10^{-14}$	10.5
2110	02-145 07:15	2	2	69	9	1	10	10	8	0	1	1	0	0	1	0	0	0	1	4	3.47318	144.0	50.4	9284.9	144	170	−37	10.4	1.9	$1.0 \cdot 10^{-13}$	10.5
2112	02-150 07:11	2	2	73	11	11	9	9	9	0	1	1	0	0	1	0	0	0	1	4	3.50044	144.3	49.8	9232.3	148	167	−40	14.1	1.9	$3.5 \cdot 10^{-13}$	10.5
2115	02-157 18:40	3	2	61	12	20	13	9	7	7	0	1	37	0	1	0	0	0	1	4	3.54089	144.7	49.0	9152.6	128	190	−29	14.1	1.9	$1.2 \cdot 10^{-12}$	10.5
2116	02-161 20:01	3	4	14	24	30	12	6	5	5	0	1	47	0	1	0	0	0	1	4	3.56225	144.9	48.6	9109.6	60	241	18	34.6	1.6	$1.3 \cdot 10^{-12}$	6.0
2117	02-164 06:28	3	3	67	20	25	3	5	6	6	0	1	43	0	1	0	0	0	1	4	3.57553	145.0	48.3	9082.6	132	190	−33	35.4	1.6	$2.8 \cdot 10^{-13}$	6.0
2118	02-168 12:55	3	2	216	9	14	1	7	7	7	0	1	36	0	1	0	0	0	1	4	3.59796	145.2	47.8	9036.5	340	335	40	43.7	1.6	$6.4 \cdot 10^{-15}$	6.0
2120	02-175 18:09	3	3	45	20	25	10	5	6	5	0	1	44	0	1	0	0	0	1	4	3.63585	145.5	47.1	8957.0	94	222	−5	35.4	1.6	$2.8 \cdot 10^{-13}$	6.0
2121	02-175 23:04	2	2	101	9	14	0	8	8	6	0	0	36	0	1	0	0	0	1	4	3.63650	145.5	47.1	8955.6	173	143	−54	28.0	1.6	$3.3 \cdot 10^{-14}$	6.0
2123	02-176 08:15	3	3	11	21	26	7	5	5	6	0	1	46	0	1	0	0	0	1	4	3.63845	145.5	47.0	8951.5	47	256	28	43.7	1.6	$1.6 \cdot 10^{-13}$	6.0
2124	02-177 10:37	3	3	46	21	26	20	8	7	6	0	1	44	0	1	0	0	0	1	4	3.64428	145.6	46.9	8939.1	96	221	−7	18.0	1.6	$4.6 \cdot 10^{-12}$	6.0
2127	02-201 00:22	2	2	101	12	5	8	9	15	0	1	1	37	31	1	0	0	0	1	4	3.76406	146.5	44.5	8672.9	158	177	−52	14.1	1.9	$1.4 \cdot 10^{-13}$	10.5
2129	02-202 23:51	3	3	75	19	24	17	7	7	6	0	1	43	0	1	0	0	0	1	4	3.77335	146.6	44.3	8651.4	117	217	−23	21.0	1.6	$1.1 \cdot 10^{-12}$	6.0
2130	02-204 06:22	1	2	95	8	5	0	9	15	0	1	0	5	23	1	0	0	0	1	4	3.78014	146.7	44.2	8635.5	145	194	−45	14.1	1.9	$7.7 \cdot 10^{-14}$	10.5
2131	02-206 04:46	3	3	31	23	29	17	9	6	6	0	1	46	0	1	0	0	0	1	4	3.78938	146.7	44.0	8613.9	56	255	23	16.9	1.8	$1.4 \cdot 10^{-11}$	8.4
2133	02-210 18:57	3	4	74	27	49	19	6	4	5	0	1	46	0	1	0	0	0	1	4	3.81203	146.9	43.6	8560.3	108	225	−17	21.4	1.9	$2.0 \cdot 10^{-11}$	10.5
2136	02-224 22:53	3	3	78	23	29	17	5	4	5	0	1	46	0	1	0	0	0	1	4	3.88001	147.4	42.2	8394.3	101	233	−11	48.9	1.6	$2.3 \cdot 10^{-13}$	6.0
2137	02-225 16:31	1	2	164	9	5	0	8	15	0	1	0	38	31	1	0	0	0	1	4	3.88357	147.4	42.2	8385.4	223	82	−40	21.4	1.9	$1.9 \cdot 10^{-14}$	10.5
2138	02-234 02:09	1	2	89	11	11	0	9	15	0	1	0	46	31	1	0	0	0	1	4	3.92300	147.7	41.4	8285.3	108	232	−16	14.1	1.9	$3.5 \cdot 10^{-13}$	10.5
2139	02-238 13:26	2	2	67	12	11	12	9	9	0	1	1	0	0	1	0	0	0	1	4	3.94393	147.8	41.0	8231.1	73	252	12	14.1	1.9	$4.1 \cdot 10^{-13}$	10.5
2140	02-240 09:22	2	2	56	9	6	8	9	12	0	1	1	0	0	1	0	0	0	1	4	3.95260	147.9	40.8	8208.4	50	268	29	14.1	1.9	$1.1 \cdot 10^{-13}$	10.5
2142	02-241 17:21	3	2	86	10	15	7	7	8	6	0	1	36	0	1	0	0	0	1	4	3.95837	147.9	40.7	8193.3	92	243	−4	34.1	1.9	$2.3 \cdot 10^{-14}$	10.5
2143	02-244 23:06	2	2	86	11	20	0	8	5	6	0	0	38	0	1	0	0	0	1	4	3.97329	148.0	40.4	8153.8	88	246	0	21.4	1.9	$2.2 \cdot 10^{-13}$	10.5
2144	02-246 01:13	3	3	74	21	27	13	5	5	5	0	1	45	0	1	0	0	0	1	4	3.97843	148.0	40.3	8140.0	71	255	13	43.7	1.6	$1.9 \cdot 10^{-13}$	6.0
2147	02-25720:03	2	2	102	9	19	0	7	5	7	0	0	38	0	1	0	0	0	1	4	4.03150	148.4	39.3	7995.6	92	247	−4	34.1	1.9	$2.4 \cdot 10^{-14}$	10.5
2148	02-258 09:43	2	2	186	8	13	0	8	8	7	0	0	34	0	1	0	0	0	1	4	4.03429	148.4	39.2	7987.9	210	101	−50	28.0	1.6	$2.4 \cdot 10^{-14}$	6.0
2150	02-261 23:01	3	3	139	20	24	13	5	5	5	0	1	44	0	1	0	0	0	1	4	4.04985	148.5	38.9	7944.4	140	218	−43	43.7	1.6	$9.8 \cdot 10^{-14}$	6.0
2153	02-284 11:50	3	2	123	9	14	3	8	8	7	0	1	36	0	1	0	0	0	1	4	4.14743	149.1	37.1	7660.8	99	249	−9	28.0	1.6	$3.3 \cdot 10^{-14}$	6.0
2154	02-287 19:41	1	2	153	10	8	0	10	15	0	1	0	9	31	1	0	0	0	1	4	4.16170	149.2	36.8	7617.7	138	225	−42	10.4	1.9	$3.7 \cdot 10^{-13}$	10.5
2155	02-295 07:26	3	2	143	12	20	23	7	5	7	0	1	37	0	1	0	0	0	1	4	4.19308	149.4	36.2	7521.2	119	240	−26	34.1	1.9	$5.2 \cdot 10^{-14}$	10.5
2156	02-302 16:31	2	3	214	23	26	26	11	9	0	1	1	5	5	1	0	0	0	1	4	4.22348	149.5	35.6	7425.6	215	104	−47	7.1	2.6	$8.6 \cdot 10^{-11}$	31.9
2157	02-305 19:50	3	2	158	11	19	11	8	7	8	0	1	36	0	1	0	0	0	1	4	4.23623	149.6	35.4	7384.9	133	232	−37	21.4	1.9	$1.7 \cdot 10^{-13}$	10.5
2158	02-309 22:10	3	3	165	20	24	7	5	7	6	0	1	42	0	1	0	0	0	1	4	4.25294	149.7	35.0	7330.9	141	225	−44	32.7	1.6	$3.1 \cdot 10^{-13}$	6.0
2160	02-319 20:01	3	3	140	20	24	20	5	6	5	0	1	42	0	1	0	0	0	1	4	4.29237	149.9	34.3	7200.9	100	254	−10	35.4	1.6	$2.4 \cdot 10^{-13}$	6.0
2162	02-320 20:09	2	2	25	8	13	0	8	8	6	0	0	34	0	1	0	0	0	1	4	4.29632	149.9	34.2	7187.7	298	55	20	28.0	1.6	$2.4 \cdot 10^{-14}$	6.0
2163	02-324 20:19	3	2	199	8	12	2	8	8	6	0	1	0	0	1	0	0	0	1	4	4.31204	150.0	33.9	7134.6	181	163	−61	28.0	1.6	$2.1 \cdot 10^{-14}$	6.0
2164	02-328 16:19	2	2	109	10	19	0	7	5	6	0	0	37	0	1	0	0	0	1	4	4.32714	150.1	33.6	7083.0	51	284	28	34.1	1.9	$2.9 \cdot 10^{-14}$	10.5
2169	02-331 23:45	3	2	173	13	21	12	8	7	6	0	1	39	0	1	0	0	0	1	4	4.33972	150.2	33.4	7039.6	139	228	−42	21.4	1.9	$3.6 \cdot 10^{-13}$	10.5
2188	03-155 03:33	3	5	134	54	53	30	13	12	5	0	1	62	0	1	0	0	0	1	3	4.93209	153.2	21.1	4371.6	250	54	−20	2.0	1.9	$4.6 \cdot 10^{-07}$	10.5
2190	03-160 05:36	3	2	173	9	13	11	8	8	6	0	1	34	0	1	0	0	0	1	4	4.94436	153.2	20.8	4298.8	304	34	30	28.0	1.6	$2.8 \cdot 10^{-14}$	6.0
2194	03-168 11:59	2	2	5	9	8	1	12	15	0	1	1	17	31	1	0	0	0	1	4	4.96423	153.3	20.3	4178.7	67	245	20	5.0	1.9	$2.8 \cdot 10^{-12}$	10.5

Table 3 (*continued*)

No.	IMP. DATE	CLN	AR	SEC	IA	EA	CA	IT	ET	EIT	EIC	IIC	PA	PET	EVD	ICP	ECP	CCP	PCP	HV	R	LON	LAT	D_{Jup}	ROT	S_{LON}	S_{LAT}	V	VEF	M	MEF
2195	03-173 07:52	3	3	66	21	27	10	5	5	5	0	1	46	0	1	0	0	0	1	4	4.97575	153.4	20.0	4107.9	151	212	−58	43.7	1.6	$1.9 \cdot 10^{-13}$	6.0
2202	03-184 14:07	2	2	77	14	6	9	9	15	0	1	1	0	0	1	0	0	0	1	4	5.00173	153.5	19.4	3944.8	163	200	−69	14.1	1.9	$2.4 \cdot 10^{-13}$	10.5
2203	03-186 08:37	2	2	14	8	13	0	7	7	7	0	0	35	0	1	0	0	0	1	4	5.00569	153.6	19.3	3919.5	71	246	16	43.7	1.6	$4.7 \cdot 10^{-15}$	6.0
2204	03-187 02:49	3	3	48	19	23	14	6	6	6	0	1	41	0	1	0	0	0	1	4	5.00738	153.6	19.2	3908.6	119	232	−29	28.0	1.6	$3.3 \cdot 10^{-13}$	6.0
2351	03-203 06:00	1	2	30	9	7	0	9	15	0	1	0	10	31	1	0	0	0	1	4	5.04312	153.8	18.3	3674.7	89	243	0	14.1	1.9	$1.3 \cdot 10^{-13}$	10.5
2371	03-238 12:14	2	2	72	8	8	10	9	11	0	1	1	0	0	1	0	0	0	1	4	5.11461	154.2	16.4	3177.3	90	249	0	14.1	1.9	$1.3 \cdot 10^{-13}$	10.5
2390	03-241 11:06	3	2	119	13	20	8	7	5	7	0	1	38	0	1	0	0	0	1	4	5.12008	154.2	16.2	3137.6	142	235	−51	34.1	1.9	$6.1 \cdot 10^{-14}$	10.5
2397	03-250 06:05	3	2	255	9	14	1	8	8	6	0	1	35	0	1	0	0	0	1	4	5.13662	154.3	15.7	3016.2	308	50	35	28.0	1.6	$3.3 \cdot 10^{-14}$	6.0
2409	03-264 20:24	1	2	188	10	2	0	9	12	0	1	0	0	0	1	0	0	0	1	4	5.16255	154.5	15.0	2822.0	189	109	−78	14.1	1.9	$6.8 \cdot 10^{-14}$	10.5
2410	03-265 11:17	3	4	73	25	49	12	9	5	5	0	1	46	0	1	0	0	0	1	4	5.16363	154.5	14.9	2813.8	27	280	58	7.8	1.9	$2.9 \cdot 10^{-10}$	10.5
2411	03-266 01:13	1	2	60	10	3	0	9	9	0	1	0	22	24	1	0	0	0	1	4	5.16472	154.5	14.9	2805.6	8	314	71	14.1	1.9	$7.8 \cdot 10^{-14}$	10.5
2418	03-279 12:24	2	2	111	8	14	0	8	8	6	0	0	36	0	1	0	0	0	1	4	5.18752	154.6	14.2	2631.1	66	261	22	28.0	1.6	$2.9 \cdot 10^{-14}$	6.0
2429	03-285 17:09	2	2	191	9	13	0	8	8	6	0	0	35	0	1	0	0	0	1	4	5.19749	154.7	13.9	2554.2	176	194	−81	28.0	1.6	$2.8 \cdot 10^{-14}$	6.0
2430	03-285 20:10	3	2	173	8	12	1	8	8	6	0	1	0	0	1	0	0	0	1	4	5.19769	154.7	13.9	2552.7	150	241	−59	28.0	1.6	$2.1 \cdot 10^{-14}$	6.0
2475	03-292 08:41	2	2	216	8	13	0	8	8	6	0	0	35	0	1	0	0	0	1	4	5.20799	154.8	13.5	2473.0	208	84	−61	28.0	1.6	$2.4 \cdot 10^{-14}$	6.0
2477	03-292 18:23	3	2	156	11	20	22	7	5	6	0	1	37	0	1	0	0	0	1	4	5.20877	154.8	13.5	2466.9	123	250	−33	34.1	1.9	$4.4 \cdot 10^{-14}$	10.5
2478	03-294 22:20	3	2	175	8	13	6	9	9	8	0	1	35	0	1	0	0	0	1	4	5.21207	154.8	13.4	2441.3	149	243	−58	21.0	1.6	$7.2 \cdot 10^{-14}$	6.0
2480	03-312 18:55	2	2	62	9	14	0	8	8	6	0	0	36	0	1	0	0	0	1	4	5.23872	155.0	12.4	2236.2	345	28	68	28.0	1.6	$3.3 \cdot 10^{-14}$	6.0
2586	03-316 21:36	3	2	222	8	12	5	7	8	6	0	1	1	22	1	0	0	0	1	4	5.24458	155.0	12.2	2191.7	209	85	−60	35.4	1.6	$9.7 \cdot 10^{-15}$	6.0
2591	03-327 14:32	2	2	62	12	21	0	8	5	6	0	0	39	0	1	0	0	0	1	4	5.25919	155.1	11.7	2083.1	341	35	65	21.4	1.9	$3.1 \cdot 10^{-13}$	10.5
2593	03-327 22:23	2	2	52	9	14	0	8	8	7	0	0	35	0	1	0	0	0	1	4	5.25969	155.1	11.7	2079.4	327	51	53	28.0	1.6	$3.3 \cdot 10^{-14}$	6.0
2594	03-329 17:35	2	2	83	9	13	0	7	8	7	0	0	35	0	1	0	0	0	1	4	5.26202	155.2	11.6	2062.5	12	310	70	35.4	1.6	$1.3 \cdot 10^{-14}$	6.0
2595	03-333 00:55	3	2	166	11	20	1	8	6	6	0	1	37	0	1	0	0	0	1	4	5.26647	155.2	11.4	2030.6	127	254	−37	21.4	1.9	$2.2 \cdot 10^{-13}$	10.5
2607	03-336 19:07	3	2	214	8	12	1	8	8	6	0	1	0	0	1	0	0	0	1	4	5.27133	155.2	11.2	1996.4	194	99	−74	28.0	1.6	$2.1 \cdot 10^{-14}$	6.0
2617	03-336 22:58	2	2	183	8	12	0	8	8	6	0	0	0	0	1	0	0	0	1	4	5.27149	155.2	11.2	1995.2	150	247	−59	28.0	1.6	$2.1 \cdot 10^{-14}$	6.0
2632	03-337 02:42	2	2	173	8	13	0	8	8	7	0	0	34	0	1	0	0	0	1	4	5.27165	155.2	11.2	1994.1	136	252	−45	28.0	1.6	$2.4 \cdot 10^{-14}$	6.0
2678	03-337 15:29	3	2	192	8	12	6	7	8	6	0	1	0	0	1	0	0	0	1	4	5.27244	155.2	11.2	1988.6	163	238	−71	35.4	1.6	$9.7 \cdot 10^{-15}$	6.0
2803	03-353 04:11	2	2	62	10	20	0	8	5	6	0	0	37	0	1	0	0	0	1	4	5.29150	155.4	10.4	1864.0	335	44	61	21.4	1.9	$1.9 \cdot 10^{-13}$	10.5
2805	03-358 16:58	3	2	155	12	20	11	9	5	7	0	1	38	0	1	0	0	0	1	4	5.29790	155.4	10.1	1826.6	106	258	−16	14.1	1.9	$1.2 \cdot 10^{-12}$	10.5
2806	03-360 07:06	3	3	166	20	26	21	5	5	5	0	1	45	0	1	0	0	0	1	4	5.29976	155.5	10.0	1816.2	121	255	−31	43.7	1.6	$1.4 \cdot 10^{-13}$	6.0
2818	04-001 13:37	2	2	197	13	13	7	10	15	0	1	1	15	31	1	0	0	0	1	4	5.30674	155.5	9.7	1779.8	163	238	−71	10.4	1.9	$1.4 \cdot 10^{-12}$	10.5
2822	04-019 12:18	3	3	108	21	26	1	5	5	6	0	1	46	0	1	0	0	0	1	4	5.32551	155.7	8.8	1706.4	33	277	54	43.7	1.6	$1.6 \cdot 10^{-13}$	6.0
2873	04-028 05:41	3	3	159	21	26	10	6	6	6	0	1	45	0	1	0	0	0	1	4	5.33380	155.8	8.3	1689.2	100	255	−10	28.0	1.6	$8.3 \cdot 10^{-13}$	6.0
2875	04-034 22:48	2	2	181	8	12	0	8	8	6	0	0	5	22	1	0	0	0	1	4	5.33996	155.8	8.0	1684.2	127	250	−36	28.0	1.6	$2.1 \cdot 10^{-14}$	6.0
2876	04-039 12:21	2	2	103	11	8	6	11	15	0	1	1	43	31	1	0	0	0	1	4	5.34403	155.9	7.8	1685.2	12	300	71	7.8	1.9	$9.3 \cdot 10^{-13}$	10.5
2877	04-046 12:19	2	2	89	8	14	0	8	8	6	0	0	36	0	1	0	0	0	1	4	5.34993	156.0	7.4	1693.3	340	34	65	28.0	1.6	$2.9 \cdot 10^{-14}$	6.0
2902	04-056 09:18	3	3	207	19	23	9	7	9	6	0	1	41	0	1	0	0	0	1	4	5.35775	156.1	6.9	1718.4	79	252	10	16.9	1.6	$2.3 \cdot 10^{-12}$	6.0
2903	04-056 22:16	3	2	143	11	20	1	8	5	6	0	1	38	0	1	0	0	0	1	4	5.35813	156.1	6.9	1720.1	349	15	73	21.4	1.9	$2.2 \cdot 10^{-13}$	10.5
2909	04-075 16:15	2	3	102	20	21	18	8	14	0	1	1	38	3	1	0	0	0	1	4	5.37128	156.2	6.0	1809.9	230	61	−39	10.4	1.9	$8.3 \cdot 10^{-12}$	10.5
2910	04-075 17:06	3	2	253	11	20	3	9	6	8	0	1	36	0	1	0	0	0	1	4	5.37128	156.2	6.0	1809.9	82	248	7	14.1	1.9	$1.0 \cdot 10^{-12}$	10.5
3008	04-087 13:21	1	2	80	8	3	0	10	15	0	1	0	45	31	1	0	0	0	1	4	5.37851	156.4	5.4	1891.5	194	66	−75	10.4	1.9	$1.2 \cdot 10^{-13}$	10.5
3010	04-097 17:23	3	2	175	8	12	4	7	8	6	0	1	34	0	1	0	0	0	1	4	5.38400	156.5	4.9	1974.0	322	43	51	35.4	1.6	$9.7 \cdot 10^{-15}$	6.0
3019	04-107 06:31	3	2	56	8	12	17	7	7	6	0	1	0	0	1	0	0	0	1	4	5.38864	156.5	4.4	2062.1	153	239	−62	43.7	1.6	$4.0 \cdot 10^{-15}$	6.0
3021	04-109 06:41	3	2	44	8	12	5	7	8	7	0	1	0	0	1	0	0	0	1	4	5.38954	156.6	4.3	2081.4	136	239	−46	35.4	1.6	$9.7 \cdot 10^{-15}$	6.0
3023	04-113 17:07	2	3	132	18	20	17	15	7	0	1	1	42	24	1	0	0	0	1	4	5.39141	156.6	4.1	2125.0	258	52	−11	7.9	4.6	$8.3 \cdot 10^{-12}$	211.2
3024	04-119 19:51	3	2	40	10	20	8	8	5	6	0	1	37	0	1	0	0	0	1	4	5.39384	156.7	3.8	2188.5	130	239	−40	21.4	1.9	$1.9 \cdot 10^{-13}$	10.5
3025	04-121 14:03	3	3	50	19	24	14	7	8	6	0	1	42	0	1	0	0	0	1	4	5.39449	156.7	3.7	2207.1	141	239	−51	19.3	1.6	$1.6 \cdot 10^{-12}$	6.0
3032	04-135 21:03	2	4	94	29	11	30	14	0	8	0	1	18	1	1	0	0	0	1	4	5.39915	156.8	3.0	2368.1	204	51	−65	2.0	1.9	$2.4 \cdot 10^{-09}$	10.5

3034	04-142 08:25	2	2	220	15	13	2	7	15	0	1	1	49	31	1	0	0	0	1	4	5.40082	156.9	2.7	2443.4	20	257	69	34.1	1.9	$3.7 \cdot 10^{-14}$	10.5
3035	04-145 04:21	2	2	230	9	5	6	10	15	0	1	1	39	31	1	0	0	0	1	4	5.40149	156.9	2.5	2478.0	34	248	55	10.4	1.9	$1.8 \cdot 10^{-13}$	10.5
3043	04-149 15:42	3	2	44	13	20	3	8	6	6	0	1	38	0	1	0	0	0	1	4	5.40244	157.0	2.3	2533.0	131	241	−40	21.4	1.9	$3.1 \cdot 10^{-13}$	10.5
3076	04-153 09:29	3	2	7	10	19	6	8	7	6	0	1	36	0	1	0	0	0	1	4	5.40315	157.0	2.1	2579.5	80	242	9	21.4	1.9	$1.5 \cdot 10^{-13}$	10.5
3082	04-153 16:55	2	2	47	13	21	0	8	5	6	0	0	40	0	1	0	0	0	1	4	5.40319	157.0	2.1	2582.6	137	242	−46	21.4	1.9	$3.6 \cdot 10^{-13}$	10.5
3897	04-166 07:26	1	2	244	8	2	0	6	12	0	1	0	0	0	1	0	0	0	1	4	5.40491	157.1	1.5	2743.6	53	245	36	43.5	1.9	$7.9 \cdot 10^{-16}$	10.5
5449	04-176 21:44	2	2	93	11	1	5	11	0	0	1	1	13	26	1	0	0	0	1	4	5.40562	157.2	0.9	2883.2	201	47	−68	7.8	1.9	$3.0 \cdot 10^{-13}$	10.5
5927	04-185 12:41	2	2	36	8	13	0	9	8	7	0	0	34	0	1	0	0	0	1	4	5.40569	157.3	0.5	2999.0	120	245	−29	22.7	1.6	$5.1 \cdot 10^{-14}$	6.0
5930	04-185 20:13	2	3	238	19	24	0	6	5	6	0	0	44	0	1	0	0	0	1	4	5.40568	157.3	0.5	3002.4	44	247	45	34.6	1.6	$1.9 \cdot 10^{-13}$	6.0
5946	04-197 19:28	2	2	218	8	13	0	8	8	6	0	0	34	0	1	0	0	0	1	4	5.40503	157.4	−0.1	3166.4	19	256	70	28.0	1.6	$2.4 \cdot 10^{-14}$	6.0
5947	04-198 02:43	3	2	47	12	20	4	7	6	7	0	1	38	0	1	0	0	0	1	4	5.40501	157.4	−0.1	3169.8	139	248	−48	34.1	1.9	$5.2 \cdot 10^{-14}$	10.5
5949	04-200 01:25	3	2	25	13	21	12	8	8	6	0	1	38	0	1	0	0	0	1	4	5.40481	157.4	−0.2	3197.5	109	246	−17	21.4	1.9	$3.6 \cdot 10^{-13}$	10.5
5952	04-201 06:22	2	2	58	8	13	0	8	8	6	0	0	35	0	1	0	0	0	1	4	5.40468	157.5	−0.3	3214.8	152	253	−61	28.0	1.6	$2.4 \cdot 10^{-14}$	6.0
5957	04-202 21:25	3	3	57	21	27	6	6	5	5	0	1	46	0	1	0	0	0	1	4	5.40449	157.5	−0.3	3237.3	151	252	−60	34.6	1.6	$5.0 \cdot 10^{-13}$	6.0
5970	04-211 08:23	2	3	85	19	20	0	10	4	14	0	0	59	0	1	0	0	0	1	4	5.40326	157.6	−0.7	3354.3	192	36	−76	5.0	1.9	$4.7 \cdot 10^{-11}$	10.5
5978	04-215 03:38	2	2	250	8	13	0	8	8	6	0	0	35	0	1	0	0	0	1	4	5.40255	157.6	−0.9	3408.7	64	248	26	28.0	1.6	$2.4 \cdot 10^{-14}$	6.0
5999	04-233 04:32	3	3	40	22	28	21	6	6	5	0	1	46	0	1	0	0	0	1	4	5.39807	157.8	−1.8	3664.2	136	255	−44	28.0	1.6	$1.4 \cdot 10^{-12}$	6.0
6001	04-234 17:12	3	4	24	29	50	21	6	8	5	0	1	46	0	1	0	0	0	1	4	5.39761	157.8	−1.9	3685.6	116	253	−24	21.4	1.9	$4.0 \cdot 10^{-11}$	10.5
6005	04-237 21:50	3	3	252	19	23	12	6	7	6	0	1	41	0	1	0	0	0	1	4	5.39657	157.8	−2.1	3732.2	102	252	−11	25.9	1.6	$4.3 \cdot 10^{-13}$	6.0
6007	04-238 01:40	2	2	92	8	13	0	7	8	6	0	0	34	0	1	0	0	0	1	4	5.39653	157.8	−2.1	3734.0	237	60	−31	35.4	1.6	$1.1 \cdot 10^{-14}$	6.0
6008	04-238 15:56	1	2	78	9	4	0	7	15	0	1	0	35	31	1	0	0	0	1	4	5.39632	157.8	−2.1	3742.9	219	57	−50	34.1	1.9	$3.2 \cdot 10^{-15}$	10.5
6012	04-244 04:23	3	3	184	19	23	6	7	5	6	0	1	41	0	1	0	0	0	1	4	5.39438	157.9	−2.4	3821.9	65	253	25	28.1	1.6	$3.2 \cdot 10^{-13}$	6.0
6020	04-254 05:10	2	3	143	19	6	18	9	15	0	1	1	37	31	1	0	0	0	1	4	5.39039	158.0	−2.9	3966.1	72	254	18	7.8	1.9	$1.6 \cdot 10^{-12}$	10.5
6024	04-263 09:07	2	2	142	9	20	0	8	5	7	0	0	37	0	1	0	0	0	1	4	5.38616	158.1	−3.3	4099.9	80	255	11	21.4	1.9	$1.6 \cdot 10^{-13}$	10.5
6027	04-266 03:58	2	2	84	9	14	0	8	8	6	0	0	36	0	1	0	0	0	1	4	5.38481	158.1	−3.5	4139.8	1	310	88	28.0	1.6	$3.3 \cdot 10^{-14}$	6.0
6030	04-270 21:33	3	2	103	8	13	3	7	8	6	0	1	34	0	1	0	0	0	1	4	5.38236	158.1	−3.7	4208.7	28	257	62	35.4	1.6	$1.1 \cdot 10^{-14}$	6.0
6032	04-271 22:37	3	3	117	21	27	14	5	5	5	0	1	46	0	1	0	0	0	1	4	5.38182	158.2	−3.7	4223.2	47	256	43	43.7	1.6	$1.9 \cdot 10^{-13}$	6.0
6036	04-280 04:15	2	2	124	13	13	13	10	15	0	1	1	41	31	1	0	0	0	1	4	5.37720	158.2	−4.2	4343.0	58	257	32	10.4	1.9	$1.4 \cdot 10^{-12}$	10.5
6040	04-287 00:23	3	2	166	15	22	19	8	7	6	0	1	40	0	1	0	0	0	1	4	5.37303	158.3	−4.5	4443.0	119	262	−28	21.4	1.9	$5.4 \cdot 10^{-13}$	10.5
6065	04-305 17:58	3	2	156	11	20	7	8	6	7	0	1	36	0	1	0	0	0	1	4	5.36030	158.5	−5.4	4713.9	107	264	−16	21.4	1.9	$2.2 \cdot 10^{-13}$	10.5
6068	04-306 11:50	3	4	168	24	30	23	6	5	5	0	1	46	0	1	0	0	0	1	4	5.35974	158.5	−5.5	4724.8	124	266	−32	34.6	1.6	$1.3 \cdot 10^{-12}$	6.0
6070	04-308 21:16	3	4	124	25	49	8	8	5	5	0	1	46	0	1	0	0	0	1	4	5.35786	158.5	−5.6	4761.1	61	260	29	10.4	1.9	$1.3 \cdot 10^{-10}$	10.5
6074	04-313 02:27	3	4	211	26	31	27	11	12	8	0	1	46	0	1	0	0	0	1	4	5.35468	158.6	−5.8	4821.1	184	11	−78	2.8	1.6	$5.9 \cdot 10^{-09}$	6.0
6075	04-313 12:46	3	3	171	19	23	2	6	6	6	0	1	41	0	1	0	0	0	1	4	5.35428	158.6	−5.8	4828.3	128	268	−36	28.0	1.6	$3.3 \cdot 10^{-13}$	6.0
6076	04-314 03:46	2	2	136	8	13	0	8	8	6	0	0	35	0	1	0	0	0	1	4	5.35379	158.6	−5.9	4837.4	79	262	12	28.0	1.6	$2.4 \cdot 10^{-14}$	6.0
6078	04-314 10:07	2	2	94	8	13	0	7	8	7	0	0	35	0	1	0	0	0	1	4	5.35359	158.6	−5.9	4841.0	19	257	71	35.4	1.6	$1.1 \cdot 10^{-14}$	6.0
6080	04-320 23:10	2	2	117	9	14	0	8	8	6	0	0	36	0	1	0	0	0	1	4	5.34831	158.6	−6.2	4935.4	53	260	38	28.0	1.6	$3.3 \cdot 10^{-14}$	6.0
6081	04-323 03:24	3	4	171	25	49	18	7	5	5	0	1	46	0	1	0	0	0	1	4	5.34642	158.7	−6.3	4968.1	128	269	−36	14.1	1.9	$6.5 \cdot 10^{-11}$	10.5
6083	04-327 16:50	2	2	68	8	14	0	8	8	7	0	0	35	0	1	0	0	0	1	4	5.34255	158.7	−6.5	5033.3	345	83	75	28.0	1.6	$2.9 \cdot 10^{-14}$	6.0
6084	04-327 16:50	2	2	137	8	14	0	8	8	6	0	0	36	0	1	0	0	0	1	4	5.34255	158.7	−6.5	5033.3	82	263	9	28.0	1.6	$2.9 \cdot 10^{-14}$	6.0
6093	04-333 07:48	3	2	200	10	14	7	7	8	6	0	1	35	0	1	0	0	0	1	4	5.33754	158.8	−6.8	5114.7	172	314	−75	35.4	1.6	$1.8 \cdot 10^{-14}$	6.0
6098	04-350 03:25	1	2	178	9	5	0	8	15	0	1	0	0	0	1	0	0	0	1	4	5.32135	158.9	−7.7	5358.3	143	278	−50	21.4	1.9	$1.9 \cdot 10^{-14}$	10.5
6101	04-361 09:48	3	2	134	10	20	1	8	5	6	0	1	37	0	1	0	0	0	1	4	5.30960	159.1	−8.2	5520.0	81	263	9	21.4	1.9	$1.9 \cdot 10^{-13}$	10.5
6106	04-363 10:48	2	2	98	8	13	0	7	8	7	0	0	35	0	1	0	0	0	1	4	5.30742	159.1	−8.3	5548.6	30	254	60	35.4	1.6	$1.1 \cdot 10^{-14}$	6.0
6107	04-364 05:00	2	2	218	12	20	0	8	5	6	0	0	39	0	1	0	0	0	1	4	5.30660	159.1	−8.4	5559.4	202	47	−63	21.4	1.9	$2.6 \cdot 10^{-13}$	10.5

4. Analysis

The most important impact parameter determined by the dust instrument is the positive charge measured on the ion-collector, Q_I, because it is relatively insensitive to noise. Fig. 4 shows the distribution of Q_I for all dust particles detected from 2000 to 2004. Ion impact charges have been detected over the entire range of six orders of magnitude in impact charge that the dust instrument can measure. Two impacts are close to the saturation limit of $\sim 10^{-8}$ C and may thus constitute lower limits of the actual impact charges. The impact charge distribution of the big particles ($Q_I > 10^{-13}$ C) follows a power law distribution with index -0.40 and is shown as a dashed line.

In the earlier 1993–1999 data sets (Papers V and VII) the impact charge distribution was reminiscent of three individual populations: small particles with impact charges $Q_I < 10^{-13}$ C (AR1), intermediate size particles with $10^{-13}\,\mathrm{C} \leqslant Q_I \leqslant 3 \times 10^{-11}$ C (AR2 and AR3) and big particles with $Q_I > 3 \times 10^{-11}$ C (AR4–AR6). This is also visible in the present data set, although somewhat less pronounced. The intermediate particles are mostly of interstellar origin and the big particles are attributed to interplanetary grains (Grün et al., 1997, see also Section 5). The majority of the small particle impacts (AR1) are due to jovian dust stream particles. A tiny fraction of the AR1 impacts occurred over the polar regions of the Sun and are attributed to interplanetary β-meteoroids (Hamilton et al., 1996; Wehry and Mann, 1999; Wehry et al., 2004).

It should be noted that the charge distribution shown in Fig. 4 is very similar to the one measured with Galileo in interplanetary space between 1993 and 1995 (i.e. between 1 and 5 AU; Paper IV). In particular, the power law index of -0.43 for the big particles was practically identical. This indicates that both dust instruments have basically detected the same dust populations in interplanetary space and that their responses to dust impacts are very similar. The only significant difference is a dip in the Ulysses charge distribution at 2×10^{-10} C (Fig. 4) which is also evident in earlier Ulysses data (Papers III, V and VII) but very weak in the Galileo data set (Paper IV). It may be due to an artefact in the Ulysses instrument electronics in AR5.

In Fig. 4 the small impacts ($Q_I < 10^{-13}$ C) which are mostly due to jovian stream particles are squeezed into two histogram bins. In order to analyse their behaviour in more detail, their number per individual digital step in ion charge amplitude is shown separately in Fig. 5. The distribution flattens for impact charges below 2×10^{-14} C. This indicates that the sensitivity threshold of the instrument may not be sharp. The impact charge distribution for these small particles with $Q_I > 2 \times 10^{-14}$ C follows a power law with index -1.9. It confirms the results from the Galileo measurements (Paper IV) that the size distribution rises steeply towards smaller particles and is much steeper than the distribution of the big particles shown in Fig. 4. However, the Galileo measurements obtained within the jovian magnetosphere give a much steeper slope of approximately -4 (Papers VI and VIII). This difference may indicate intrinsic differences in the size distribution of the jovian stream particles in the jovian magnetosphere as compared to interplanetary space.

The ratio of the channeltron charge Q_C and the ion-collector charge Q_I is a measure of the channeltron amplification A, which in turn is an important parameter for dust impact identification (Paper I). In Fig. 6 we show the charge ratio Q_C/Q_I as a function of Q_I for the 2000–2004 dust impacts with the channeltron high voltage set to 1250 V (HV = 4). This diagram is directly comparable with similar diagrams in the previous Papers III, V and VII, although they were for the lower voltage HV = 3.

The mean amplification determined from particles with $10^{-12}\,\mathrm{C} \leqslant Q_I \leqslant 10^{-11}$ C and HV = 4 is $A \simeq 1.4$. Although this is up to 40% lower than the values derived from the data with the lower voltage before 2000, a sufficiently high channeltron amplification could be achieved with this higher voltage to maintain stable instrument operation. It shows that the channeltron degradation could be mostly counterbalanced by increasing the high voltage by one digital step. Much more severe electronics degradation was found for the Galileo dust detector during Galileo's orbital tour in the jovian system. It was probably related to the harsh radiation environment in the magnetosphere of the giant planet (Krüger et al., 2005b).

In Fig. 7 we show the masses and velocities of all dust particles detected between 2000 and 2004. As in the period before 2000, velocities occur over the entire calibrated range from 2 to 70 km s^{-1}. The masses vary over 10 orders of magnitude from 10^{-6} to 10^{-16} g. The mean errors are a factor of 2 for the velocity and a factor of 10 for the mass. The clustering of the velocity values is due to discrete steps in the rise time measurement but this quantisation is much smaller than the velocity uncertainty. For many particles in the lowest two amplitude ranges (AR1 and AR2) the velocity had to be computed from the ion charge signal alone which leads to the vertical striping in the lower mass range in Fig. 7 (most prominent above 10 km s^{-1}). In the higher amplitude ranges the velocity could normally be calculated from both the target and the ion charge signal, resulting in a more continuous distribution in the mass–velocity plane. Impact velocities below about 3 km s^{-1} should be treated with caution because anomalous impacts onto the sensor grids or structures other than the target generally lead to prolonged rise times and hence to unnaturally low impact velocities.

Masses and velocities in the lowest amplitude range (AR1, particles indicated by plus signs) should be treated with caution. These are mostly jovian stream particles (Section 5.2) for which we have clear indications that their masses and velocities are outside the calibrated range of the dust instrument (Zook et al., 1996). The grains are probably much faster and smaller than implied by Fig. 7.

5. Discussion

In Fig. 8 we show the dust impact rate detected in various amplitude ranges together with the total impact rate summed over all amplitude ranges. The highest total impact rate was recorded in June 2004 when Ulysses was about 1.3 AU away from Jupiter. It was dominated by Jupiter dust stream particles which occurred in the lowest amplitude range AR1. At ecliptic plane crossing in 2001 another maximum in the total impact rate coincided with a peak in the rate of bigger particles in the three highest ion amplitude ranges (AR4–AR6). These impacts are attributed to interplanetary particles on low inclination orbits (Grün et al., 1997). They are the impacts with $Q_I > 10^{-10}$ C shown in Fig. 4. The impact rate of intermediate sized particles in AR2 and AR3 showed relatively little variation. This size range is dominated by interstellar impactors. Details of the various dust populations are discussed below and summarised in Table 4.

Fig. 9 shows the sensor orientation at the time of a particle impact (rotation angle). The big particles (diamonds, impact charge $Q_I \geqslant 8 \times 10^{-14} C$ which roughly corresponds to AR2-6) are concentrated towards the upstream direction of interstellar helium (cf. Fig. 10, bottom panel Witte et al., 1996). They have been detected with a relatively constant rate during the entire four-year period (Fig. 8). The particles with the highest ion amplitude ranges (AR4–AR6) are not distinguished in this diagram because they cannot be separated from interstellar particles by directional arguments alone. They have to be distinguished by other means (e.g. mass and speed). In addition, their total number is so small that they constitute only a small 'contamination' of the interstellar particles in Fig. 9. In the ecliptic plane at 1.3 AU, however, interplanetary particle flux dominates over interstellar flux by a factor of about 3 (in number).

Many of the small particles detected before November 2002 (crosses, $Q_I \leqslant 8 \times 10^{-14}$ C roughly corresponding to AR1) are also compatible with the interstellar direction and a few of them have been detected over the Sun's polar regions. Since November 2002, however, the majority of the small grains are roughly compatible with the line-of-sight direction towards Jupiter (Fig. 11) and they are jovian dust stream particles.

5.1. Interplanetary dust

Fig. 10 shows the data from Ulysses' launch until the end of 2004 and compares them with two meteoroid environment models by Divine (1993) and Staubach et al. (1997). For most of the mission time, excluding the ecliptic plane crossings in 1995 and 2001, the Divine model predicts impacts from a very broad range of directions, with spin angles from 45° to 300°. The impactors belong mostly to the so-called 'halo' population which was introduced in the model to explain the Pioneer 10 and 11 data (Divine, 1993). The Ulysses directional impacts had not been available at the time of construction of the model, and they do not confirm that the 'halo' population can exist. In contrast, the Staubach et al. (1997) model was fitted to more Ulysses data than the Divine model, taking the directional information into account. It is in better agreement with the data, placing most of the impacts into the spin angle range from 30° to 120°. Most of the impacts are due to the interstellar dust flowing through the solar system (Grün et al., 1994).

One more observation from these plots is that the Divine and Staubach models predict higher flux during the ecliptic plane crossings than the data permit. The time dependence of the interstellar dust flux was asserted after the meteoroid models under review had been constructed (Landgraf, 2000). However, the disagreement at the ecliptic plane

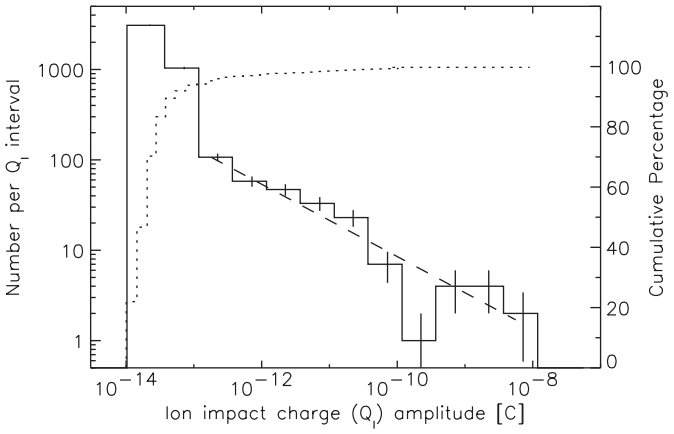

Fig. 4. Distribution of the impact charge amplitude Q_I for all dust particles detected from 2000 to 2004. The solid line indicates the number of impacts per charge interval, and the dotted line shows the cumulative percentage. Vertical bars indicate the $\sqrt{n}$ statistical fluctuation. A power law fit to the data with $Q_I > 10^{-13}$ C is shown as a dashed line (number $N \sim Q_I^{-0.40}$).

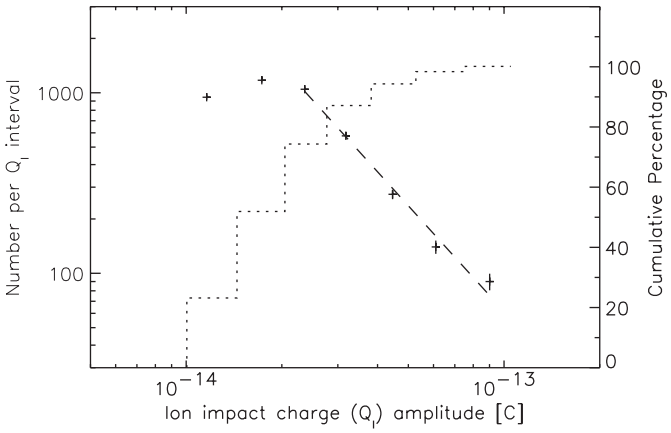

Fig. 5. Same as Fig. 4 but for the small particles in the lowest amplitude range (AR1) only. A power law fit to the data with 2×10^{-14} C $< Q_I < 10^{-13}$ C is shown as a dashed line (number $N \sim Q_I^{-1.9}$).

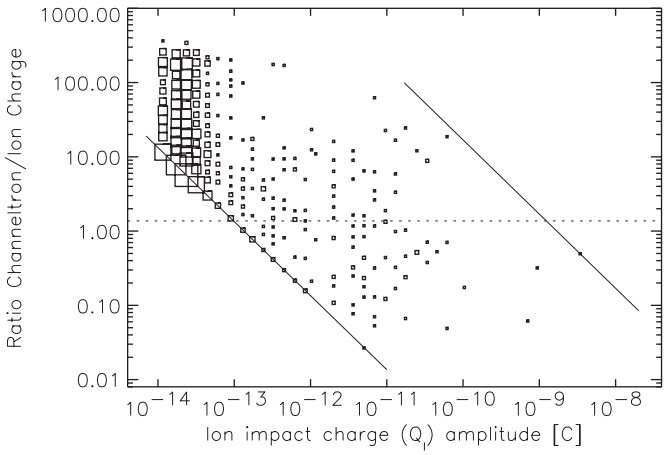

Fig. 6. Channeltron amplification factor $A = Q_C/Q_I$ as a function of impact charge Q_I for all dust impacts detected between 2000 and 2004 with channeltron voltage set to HV = 4. The solid lines denote the sensitivity threshold (lower left) and the saturation limit (upper right) of the channeltron. Squares indicate dust particle impacts. The area of each square is proportional to the number of events included (the scaling of the squares is not the same as in earlier papers). The dotted horizontal line shows the mean value of the channeltron amplification $A = 1.4$ for ion impact charges $10^{-12}\text{C} < Q_I < 10^{-11}\text{C}$.

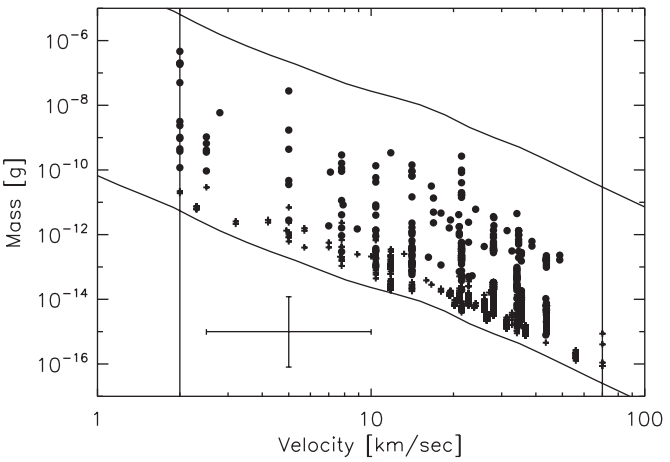

Fig. 7. Masses and impact velocities of all impacts recorded with the Ulysses sensor from 2000 to 2004. The lower and upper solid lines indicate the threshold and the saturation limit of the detector, respectively, and the vertical lines indicate the calibrated velocity range. A sample error bar is shown that indicates a factor of 2 uncertainty for the velocity and a factor of 10 for the mass determination. Note that the small particles (plus signs) are most likely much faster and smaller than implied by this diagram (see text for details).

crossings was not anticipated, since almost all data incorporated in the models were taken from the ecliptic plane. Possible explanations of the discrepancy are the roughness of model fits as well as different representations of the data taken for model adjustments and displayed in Fig. 10. Divine (1993) reported the accuracy of fits to spacecraft data of 25% on average, with the worst mismatches of up to 50%. While Fig. 10 selects all impacts above a fixed threshold of charge released, the models were fitted using more uncertain inferred mass thresholds. The inference of mass is based on speed determination that is uncertain by a factor of 2.

5.2. Jupiter dust streams

In 1992/1993—during Ulysses' first Jupiter flyby—a total of 11 burst-like dust streams originating from the Jupiter system were measured within 2 AU from the planet and maximum impact rates up to 2000 per day exceeded—by three orders of magnitude—the impact rates typically measured in interplanetary space. The data implied strong electromagnetic interaction also with the solar wind-driven interplanetary magnetic field. No dust streams were detected in 1998 (Krüger et al., 2001b) when Ulysses was at aphelion but Jupiter was on the opposite side of the Sun, providing conclusive proof that the jovian system is the source.

During Ulysses' second Jupiter flyby, the first dust stream was detected in November 2002 at a jovicentric distance of 3.4 AU (Fig. 11), beating Ulysses' previous 2 AU record. Unfortunately, on 1 December 2002, a few days after onset of this very distant stream, the instrument was switched off for power saving on board the spacecraft (Table 1), so that the end of the stream could not be measured. The instrument was switched on again on 3 June 2003 when Ulysses was only 2 AU away from Jupiter. Additional switch-offs occurred between 26 March and 8 April 2002 (14 days), from 28 June through 22 August 2003 (25 days) and between 30 November and 2 December 2004 (2 days).

A total of 22 streams were detected by December 2004 which is twice the number of streams measured during the 1992 flyby. During 10 of the identified streams, the impact rates exceeded 100 per day. In summer 2004, a particularly strong dust burst occurred with rates above 2000 per day (Fig. 11), containing many more particle impacts than all of the other streams combined (Table 2). This dust burst was the strongest dust emission measured during the distant Jupiter flyby and the second largest dust stream flux seen in interplanetary space. It was exceeded only by the fluxes measured by Galileo during approach to Jupiter in 1995. Interestingly, this burst was detected close to the jovian equator at about 1.3 AU jovicentric distance. Near Jupiter closest approach of 0.8 AU, when the spacecraft was at a jovigraphic latitude of $+50^\circ$, the rates were about an order of magnitude lower. Note that the dust impact rate varied by more than 4 orders of magnitude and the streams were detected from 0.8 AU jovicentric distance out to beyond 3 AU. Ulysses dust stream detections continue into 2005 and a detailed analysis of this data set has been given by Krüger et al. (2006b).

Strong periodicities of the streams are evident in Fig. 11: between mid-2003 and early-2004, the streams occurred with roughly the solar rotation period which is about 26 days. In mid-2004—when Ulysses was close to the jovian

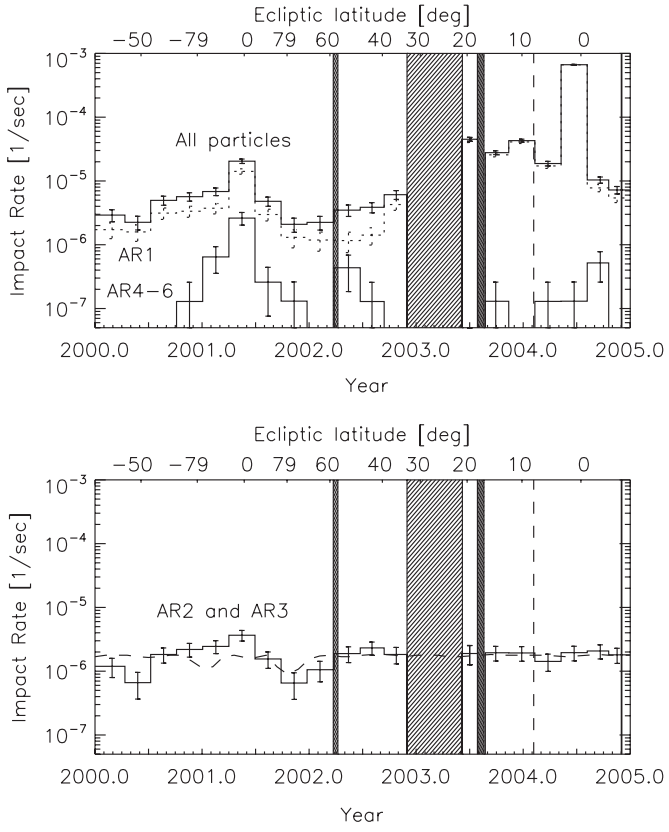

Fig. 8. Impact rate of dust particles detected with the Ulysses dust sensor as a function of time. The ecliptic latitude of the spacecraft is indicated at the top. Shaded areas indicate periods when the dust instrument was switched off. The switch-off for 2 days in December 2004 has been ignored for impact rate calculation. Jupiter closest approach is indicated by a vertical dashed line. Upper panel: total impact rate (upper solid histograms), impact rate of small particles (AR1, dotted histograms), and impact rate of big particles (AR4–AR6, lower solid histograms). Note that a rate of about 10^{-7} impacts per second is caused by a single dust impact in the averaging interval of about 90 days. An averaging interval of only 55 days had to be used for the time interval June and July 2003 because the instrument was switched off before and after this period. Lower panel: impact rate of intermediate size particles (AR2 and AR3, solid histograms). A model for the rate of interstellar particles assuming a constant flux is superimposed as a dashed line. Vertical bars indicate the $\sqrt{n}$ statistical fluctuation.

equatorial plane—the streams occurred at about half this period, while at the end of 2004 the period had doubled again. This behaviour was predicted by Hamilton and Burns (1993).

The rotation angle for each dust impact is shown in the bottom panel of Fig. 11. Contour lines are superimposed which indicate the effective dust sensor area for particles approaching the spacecraft from the line-of-sight direction to Jupiter. Grains approaching on straight trajectories from a source in the Jupiter system should arrive from close to the line-of-sight direction to the planet, while the directions of particles interacting with the interplanetary magnetic field can differ significantly (Zook et al., 1996).

Many dust streams can easily be recognised as vertical bands lying approximately in the line-of-sight direction to Jupiter. A few streams, however, strongly deviated from this direction. This is particularly evident for the stream measured in November 2002 at 3.4 AU from Jupiter and

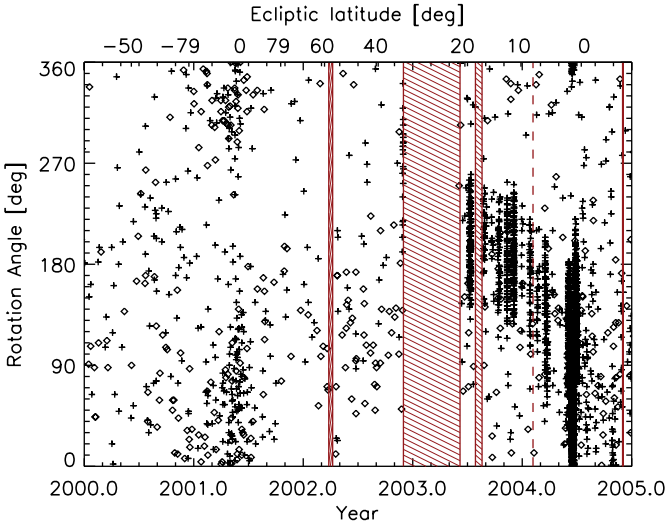

Fig. 9. Rotation angle vs. time for all particles detected in the 2000–2004 interval. Plus signs indicate particles with impact charge $Q_1 < 10^{-13}$ C (AR1), diamonds those with $Q_1 > 10^{-13}$ C (AR2–AR6). Ulysses' ecliptic latitude is indicated at the top.

Table 4
Physical parameters of major dust populations

Population[a]	Mass (g)[b]	Radius (μm)[c]	Impact speed (km s^{-1})[d]	Source[e]	Reference[f]
Jovian dusts streams	$\approx 10^{-17}$[g]	~0.01[g]	>200[g]	Io	Zook et al. (1996)
Interplanetary dust	10^{-15}–10^{-6}	0.05–50	3–50	Comets/asteroids	Grün et al. (1997)
Interstellar dust	10^{-15}–10^{-11}	0.05– 1	> 26	Local interstellar cloud	Frisch et al. (1999)

[a]Detected by Ulysses in interplanetary space.
[b]The measured mass range.
[c]Typical particle sizes assuming spherical particles with density 2000 kg m^{-3}.
[d]Measured impact speeds.
[e]The source for the majority of grains.
[f]References where these parameters are derived.
[g]Derived from dynamical modelling.

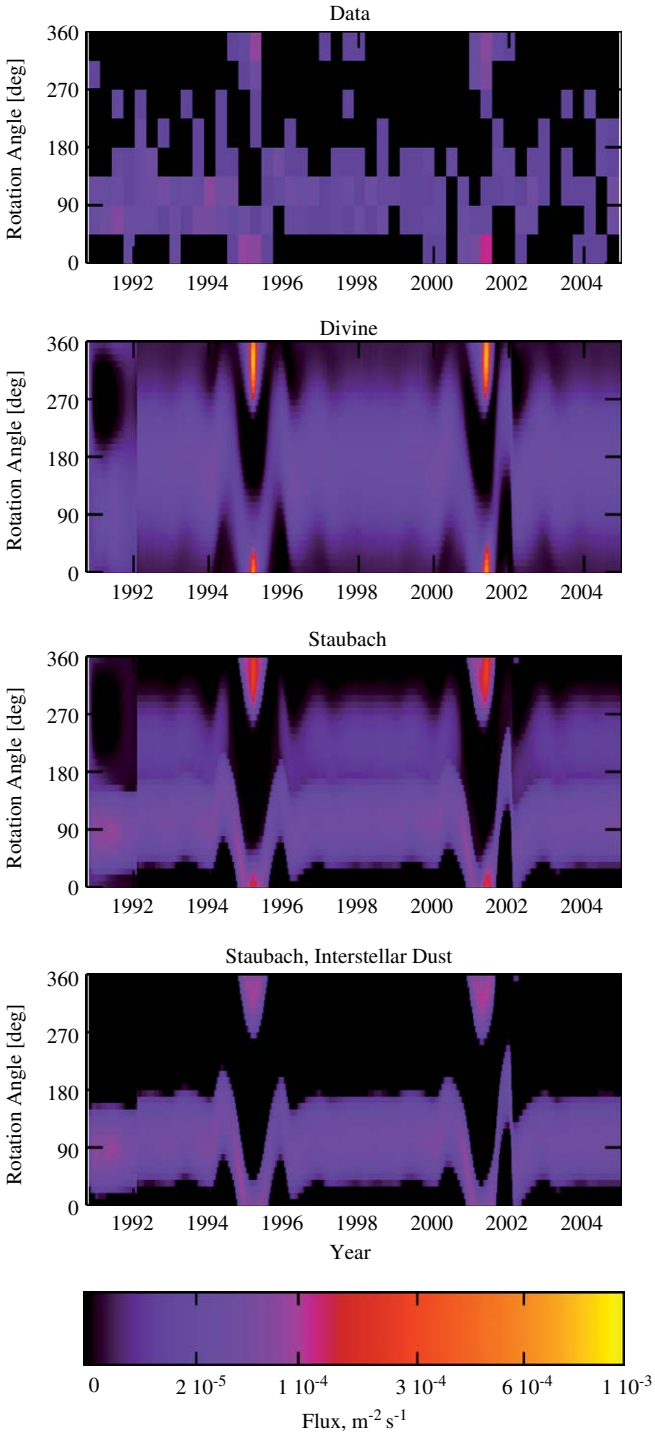

Fig. 10. Particle fluxes onto the Ulysses dust detector as seen in the data (AR3–AR6; top panel) and predicted by the meteoroid environment models by Divine (1993, second panel) and Staubach et al. (1997, third panel). The bottom panel shows the interstellar population only. The Jupiter encounter in 1992 is best seen on the model plots as a sharp swing in directionality of impacts caused by the rotation of spacecraft velocity relative to the giant planet. The two ecliptic plane crossings near the perihelion in 1995 and 2001 are marked by the high impact rates due to the number density of dust increase near the Sun and high speed of Ulysses relative to this dust. As the spacecraft moved north at the times of the crossings, the meteoroids came from the ecliptic north as well (spin angle 0).

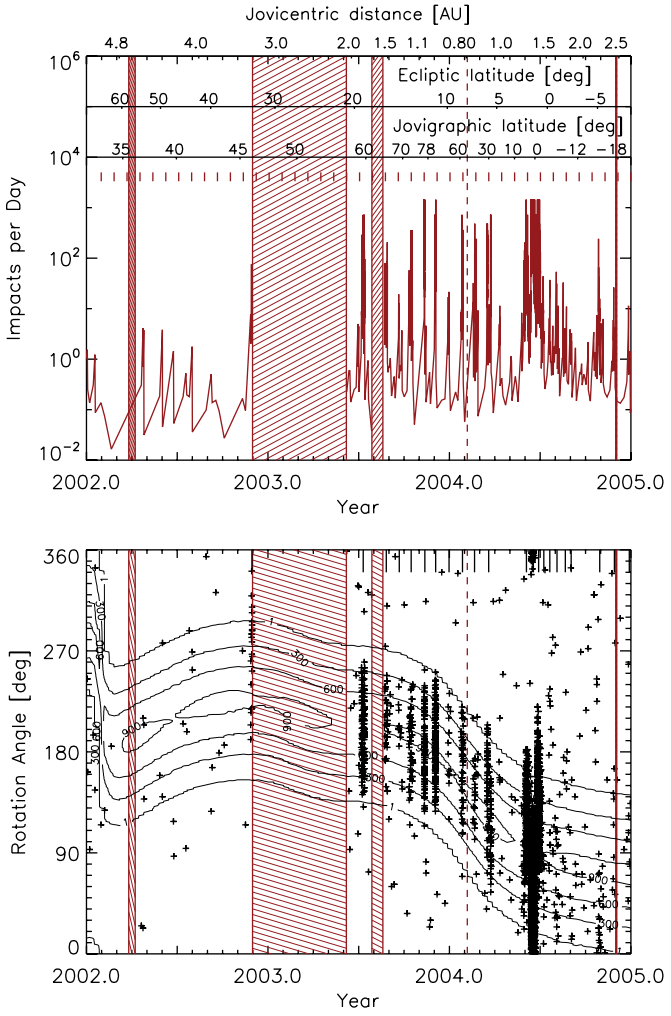

Fig. 11. Ulysses dust stream measurements from 2002 to 2004 (AR1). *Top panel:* impact rate. No smoothing was applied to the data. The distance from Jupiter, ecliptic latitude and declination w.r.t. Jupiter (jovigraphic latitude), respectively, are shown at the top. Short vertical dashes indicate the solar rotation period. A vertical dashed line shows Jupiter closest approach on 5 February 2004 and three grey shaded areas indicate periods when the dust instrument was switched off. *Bottom panel:* impact direction (rotation angle; ecliptic north is at 0°). Each cross indicates an individual dust particle impact. Contour lines show the effective dust sensor area for particles approaching from the line-of-sight direction to Jupiter and vertical dashes at the top indicate the dust streams.

for the burst detected in June/July 2004. For each stream, the measured range in rotation angle scatters over more than 100°, consistent with the wide field of view of the dust sensor. In the time interval considered in this paper, due to the orientation of the spacecraft spin axis w.r.t. Jupiter, the dust sensor had almost its maximum sensitive area exposed to grains approaching from the Jupiter direction. The impact direction of the streams is correlated with the polarity and strength of the interplanetary magnetic field (Krüger et al., 2005a). Furthermore, the occurrence of the dust streams appears to be correlated with corotating interaction regions (CIRs; Flandes and Krüger, 2006)

which are compressed, high-speed solar wind regions characterised by enhanced magnetic field strength. Similar correlations were also reported for the dust streams at Jupiter and Saturn (Grün et al., 1993; Kempf et al., 2005). During both Jupiter flybys (1991–1992 and 2002–2004) the Ulysses spacecraft has been an exceptionally successful dust stream detector finding streams over a large latitude range from below the equator to the north polar region of Jupiter (-35° to $+75^\circ$ jovigraphic latitude).

5.3. Interstellar dust

Interstellar particles move on hyperbolic trajectories through the solar system and approach Ulysses from the same direction as the interstellar gas (Grün et al., 1994; Baguhl et al., 1995a; Witte et al., 1996). They can therefore be identified by their impact direction and their impact speed. In the Ulysses and Galileo dust data sets interstellar impactors are mostly found in amplitude ranges AR2 and AR3.

In the 1993–1999 interval the impact rate of interstellar grains varied by about a factor of 2.5: between 1993 and 1995 the rate was $\sim 2 \times 10^{-6}\,\mathrm{s}^{-1}$ (Paper V) while in the 1996 to 1999 interval it dropped to $\sim 8 \times 10^{-7}\,\mathrm{s}^{-1}$ (Paper VII). Between 2000 and 2004 the average impact rate was again $\sim 2 \times 10^{-6}\,\mathrm{s}^{-1}$ (bottom panel of Fig. 8). However, one should keep in mind that in 2003/04 AR2 may contain jovian stream particles (Section 5.2) which may lead to a somewhat increased impact rate in this time interval. The maximum at ecliptic plane crossing in early-2001 also indicates some contribution from interplanetary impactors.

Fig. 8 also shows the expected impact rate of interstellar particles assuming that they approach from the direction of interstellar helium (Witte et al., 1996) and that they move through the solar system on straight trajectories with a relative velocity of $26\,\mathrm{km\,s}^{-1}$. This assumption means dynamically that radiation pressure cancels gravity for these particles ($\beta = 1$) and that their Larmor radii are large compared with the dimension of the solar system. Both assumptions are reasonable for particles with masses between 10^{-13} and $10^{-12}\,\mathrm{g}$ which is the dominant size range measured for interstellar grains (Grün et al., 1997). The variation predicted by the model is caused by changes in the instrument's viewing direction with respect to the approach direction of the particles and changes in the relative velocity between the spacecraft and the particles. The dust particle flux is independent of heliocentric distance in this simple model, which gives relatively good agreement with the observed impact rate.

A more detailed modelling of the dynamics of the electrically charged dust grains in the heliosphere can give us information about the LIC where the particles originate from. In the time interval 2001–2004 the interstellar dust flux stayed relatively constant, in agreement with improved models (Landgraf et al., 2003). The models predict a rather constant flux until 2008. The dominant contribution to the flux comes from grains with a charge to mass ratio $q/m = 0.59\,\mathrm{C\,kg}^{-1}$ and $\beta = 1.1$ which—in the simulation—corresponds to a grain radius of $0.3\,\mu\mathrm{m}$. The fact that the models fit the flux variation assuming a constant dust concentration in the LIC implies that the dust phase of the LIC is homogeneously distributed over length scales of at least 50 AU, the distance inside the LIC traversed by the Sun while Ulysses was measuring the interstellar dust inside the heliosphere.

Ulysses also monitored interstellar dust at high ecliptic latitudes between 3 and 5 AU. Dust measurements between 0.3 and 3 AU in the ecliptic plane exist also from Helios, Galileo and Cassini. This data show evidence for distance-dependent alteration of the interstellar dust stream caused by radiation pressure, gravitional focussing and electromagnetic interaction with the time-varying interplanetary magnetic field (Altobelli et al., 2003, 2005a,b).

In a recent re-analysis of the Ulysses interstellar dust data Altobelli et al. (2004) found that impacts onto the inner sensor side wall give impact signals not distinguishable from impacts onto the sensor target and that the side wall is almost as sensitive to dust impacts as the target. Similar results were also found in laboratory experiments (Willis et al., 2004, 2005). This shows that wall impacts have to be taken into account for estimating the intrinsic velocity dispersion of interstellar impactors. Neglect of the sensor side wall overestimates the interstellar dust stream velocity dispersion by about 30% and the interstellar dust flux by about 20%.

5.4. β-meteoroids

Maxima in the impact rate of the smallest particles (AR1) occurred at the ecliptic plane crossings in 1995 (Paper V) and 2001 (upper panel in Fig. 8). Although in both cases the maximum was reached during a short period around ecliptic plane crossing, many particles were also detected at high ecliptic latitudes. These grains are attributed to a population of submicron-sized interplanetary particles whose dynamics is dominated by solar radiation pressure. They move on escape trajectories from the solar system (Baguhl et al., 1995b; Hamilton et al., 1996, β-meteoroids). β-meteoroids were identified with Ulysses over the Sun's poles in 1994–1995 (Wehry and Mann, 1999) and 2000/01 (Wehry et al., 2004). Due to the detection geometry, however, they became undetectable outside these periods, explaining the lower impact rates in AR1. β-meteoroids will become detectable again from end 2006 until 2008.

6. Summary

In this paper, which is the ninth in a series of Ulysses and Galileo papers, we present data from the Ulysses dust instrument for the period January 2000 to December 2004. In this time interval the spacecraft almost completed an entire revolution about the Sun in the heliocentric distance

range between 1.3 and 5.4 AU. In February 2004, the spacecraft approached Jupiter to 0.8 AU.

A total number of 4415 dust impacts were recorded during this period. Together with 1695 impacts recorded in interplanetary space and near Jupiter between Ulysses' launch in October 1990 and December 1999 (Grün et al., 1995a; Krüger et al., 1999b, 2001b), the complete data set of dust impacts measured with the Ulysses dust detector so far comprises 6110 impacts.

A relatively constant impact rate of 0.3 per day was detected during the first three years (2000–2002) with a peak of about 1.5 per day at ecliptic plane crossing in early-2001. From 2000–2002 most of these particles were of interstellar origin, a minor fraction being interplanetary particles. The measurements from the entire Ulysses mission since launch in 1990 give good agreement with the interplanetary flux model of Staubach et al. (1997) and are inconsistent with Divine's 1993 model.

Since 2003 jovian dust stream particles dominated the overall impact rate, reaching a maximum of about 2000 per day in June/July 2004. The dust stream data imply strong coupling of the grains to the interplanetary magnetic field.

Noise tests performed regularly during the five-year period showed a degradation in the noise sensitivity of the dust instrument which was caused by a reduction in the channeltron amplification. The channeltron voltage had to be raised once to counterbalance this degradation which, however, had no effect on the interpretation of the present data set.

Acknowledgements

We thank the Ulysses project at ESA and NASA/JPL for effective and successful mission operations. This work has been supported by the Deutsches Zentrum für Luft- und Raumfahrt e.V. (DLR) under Grants 50 0N 9107 and 50 QJ 9503. Support by Max-Planck-Institut für Kernphysik and Max-Planck-Institut f́ur Sonnensystemforschung is also gratefully acknowledged.

Appendix A. Supplementary data

Supplementary data associated with this article can be found in the online version, at 10.1016/j.pss.2006.04.015.

References

Altobelli, N., Kempf, S., Landgraf, M., Srama, R., Dikarev, V., Krüger, H., Moragas-Klostermeyer, G., Grün, E., 2003. Cassini between Venus and Earth: detection of interstellar dust. J. Geophys. Res. 108 (A10), 7–1.

Altobelli, N., Moissl, R., Krüger, H., Landgraf, M., Grün, E., 2004. Influence of wall impacts on the Ulysses dust detector in modelling the interstellar dust flux. Planetary Space Sci. 52, 1287–1295.

Altobelli, N., Kempf, S., Krüger, H., Landgraf, M., Srama, R., Grün, E., 2005a. in: AIP Conference Proceedings 761: The Spectral Energy Distributions of Gas-Rich Galaxies: Confronting Models with Data, pp. 149–152.

Altobelli, N., Kempf, S., Krüger, H., Landgraf, M., Roy, M., Grün, E., 2005b. Interstellar dust flux measurements by the Galileo dust instrument between Venus and Mars orbit. J. Geophys. Res. 110, 7102–7115.

Baggaley, W.J., Neslušan, L., 2002. A model of the heliocentric orbits of a stream of Earth-impacting interstellar meteoroids. Astron. Astrophys. 382, 1118–1124.

Baguhl, M., Grün, E., Linkert, G., Linkert, D., Siddique, N., 1993. Identification of 'small' dust impacts in the Ulysses dust detector data. Planetary Space Sci. 41, 1085–1098.

Baguhl, M., Grün, E., Hamilton, D.P., Linkert, G., Riemann, R., Staubach, P., 1995a. The flux of interstellar dust observed by Ulysses and Galileo. Space Sci. Rev. 72, 471–476.

Baguhl, M., Hamilton, D.P., Grün, E., Dermott, S.F., Fechtig, H., Hanner, M.S., Kissel, J., Lindblad, B.A., Linkert, D., Linkert, G., Mann, I., McDonnell, J.A.M., Morfill, G.E., Polanskey, C., Riemann, R., Schwehm, G.H., Staubach, P., Zook, H.A., 1995b. Dust measurements at high ecliptic latitudes. Science 268, 1016–1020.

Balogh, A., Marsden, R., Smith, E.E., 2001. The Heliosphere Near Solar Minimum: The Ulysses Perspective. Springer Praxis, Springer, Berlin, Heidelberg, New York.

Czechowski, A., Mann, I., 2003. Penetration of interstellar grains into the heliosphere. J. Geophys. Res. 108 (A10), 8038, 10.1029/2003JA009917.

Dikarev, V., Landgraf, M., Grün, E., Baggaley, W., Galligan, D., 2001. Interplanetary dust model: from micron sized dust to meteors. Proceedings of the Meteroids 2001 Conference, pp. 609–615.

Dikarev, V., Jehn, R., Grün, E., 2002. Towards a new model of the interplanetary metereoroid environment. Adv. Space Res. 29 (8), 1171–1175.

Divine, N., 1993. Five populations of interplanetary meteoroids. J. Geophys. Res. 98, 17029–17048.

Flandes, A., Krüger, H., 2006. CIR modulation of Jupiter dust stream detection. In: Proceedings of the Conference Dust in Planetary System, held in Kaua'i, Hawaii, September, 2005. in press.

Frisch, P.C., Slavin, J.D., 2003. The Chemical Composition and Gas-to-Dust Mass Ratio of Nearby Interstellar Matter. Astrophys. J. 594, 844–858.

Frisch, P.C., Dorschner, J., Geiß, J., Greenberg, J.M., Grün, E., Landgraf, M., Hoppe, P., Jones, A.P., Krätschmer, W., Linde, T.J., Morfill, G.E., Reach, W.T., Slavin, J., Svestka, J., Witt, A., Zank, G.P., 1999. Dust in the local interstellar wind. Astrophys. J. 525, 492–516.

Graps, A.L., Grün, E., Svedhem, H., Krüger, H., Horányi, M., Heck, A., Lammers, S., 2000. Io as a source of the Jovian dust streams. Nature 405, 48–50.

Grün, E., Landgraf, M., 2000. Collisional consequences of big interstellar grains. J. Geophys. Res. 105 (A5), 10,291–10,298.

Grün, E., Fechtig, H., Hanner, M.S., Kissel, J., Lindblad, B.A., Linkert, D., Maas, D., Morfill, G.E., Zook, H.A., 1992a. The Galileo dust detector. Space Sci. Rev. 60, 317–340.

Grün, E., Fechtig, H., Kissel, J., Linkert, D., Maas, D., McDonnell, J.A.M., Morfill, G.E., Schwehm, G.H., Zook, H.A., Giese, R.H., 1992b. The Ulysses dust experiment. Astron. Astrophys. Suppl. 92, 411–423.

Grün, E., Zook, H.A., Baguhl, M., Balogh, A., Bame, S.J., Fechtig, H., Forsyth, R., Hanner, M.S., Horányi, M., Kissel, J., Lindblad, B.A., Linkert, D., Linkert, G., Mann, I., McDonnell, J.A.M., Morfill, G.E., Phillips, J.L., Polanskey, C., Schwehm, G.H., Siddique, N., Staubach, P., Svestka, J., Taylor, A., 1993. Discovery of Jovian dust streams and interstellar grains by the Ulysses spacecraft. Nature 362, 428–430.

Grün, E., Gustafson, B.E., Mann, I., Baguhl, M., Morfill, G.E., Staubach, P., Taylor, A., Zook, H.A., 1994. Interstellar dust in the heliosphere. Astron. Astrophys. 286, 915–924.

Grün, E., Baguhl, M., Divine, N., Fechtig, H., Hamilton, D.P., Hanner, M.S., Kissel, J., Lindblad, B.A., Linkert, D., Linkert, G., Mann, I., McDonnell, J.A.M., Morfill, G.E., Polanskey, C., Riemann, R., Schwehm, G.H., Siddique, N., Staubach, P., Zook, H.A., 1995a.

Two years of Ulysses dust data. Planetary Space Sci. 43, 971–999 Paper III.

Grün, E., Baguhl, M., Divine, N., Fechtig, H., Hamilton, D.P., Hanner, M.S., Kissel, J., Lindblad, B.A., Linkert, D., Linkert, G., Mann, I., McDonnell, J.A.M., Morfill, G.E., Polanskey, C., Riemann, R., Schwehm, G.H., Siddique, N., Staubach, P., Zook, H.A., 1995b. Three years of Galileo dust data. Planetary Space Sci. 43, 953–969 Paper II.

Grün, E., Baguhl, M., Hamilton, D.P., Kissel, J., Linkert, D., Linkert, G., Riemann, R., 1995c. Reduction of Galileo and Ulysses dust data. Planetary Space Sci. 43, 941–951 Paper I.

Grün, E., Staubach, P., Baguhl, M., Hamilton, D.P., Zook, H.A., Dermott, S.F., Gustafson, B.A., Fechtig, H., Kissel, J., Linkert, D., Linkert, G., Srama, R., Hanner, M.S., Polanskey, C., Horányi, M., Lindblad, B.A., Mann, I., McDonnell, J.A.M., Morfill, G.E., Schwehm, G.H., 1997. South–North and radial traverses through the interplanetary dust cloud. Icarus 129, 270–288.

Grün, E., Krüger, H., Graps, A., Hamilton, D.P., Heck, A., Linkert, G., Zook, H., Dermott, S.F., Fechtig, H., Gustafson, B., Hanner, M., Horányi, M., Kissel, J., Lindblad, B., Linkert, G., Mann, I., McDonnell, J.A.M., Morfill, G.E., Polanskey, C., Schwehm, G.H., Srama, R., 1998. Galileo observes electromagnetically coupled dust in the Jovian magnetosphere. J. Geophys. Res. 103, 20011–20022.

Grün, E., Krüger, H., Landgraf, M., 2001. In: Balogh, A., Marsden, R., Smith, E. (Eds.), The Heliosphere at Solar Minimum: The Ulysses Perspective. Springer, Praxis, pp. 373–404.

Hamilton, D.P., Burns, J.A., 1993. Ejection of dust from Jupiter's gossamer ring. Nature 364, 695–699.

Hamilton, D.P., Grün, E., Baguhl, M., 1996. in: Gustafson, B.A.S., Hanner, M.S. (Eds.), Physics, Chemistry and Dynamics of Interplanetary Dust, ASP Conference Series, vol. 104, pp. 31–34.

Horányi, M., Morfill, G.E., Grün, E., 1993. Mechanism for the acceleration and ejection of dust grains from Jupiter's magnetosphere. Nature 363, 144–146.

Horányi, M., Grün, E., Heck, A., 1997. Modeling the Galileo dust measurements at Jupiter. Geophys. Res. Lett. 24, 2175–2178.

Jones, G.H., Balogh, A., 2003. A survey of strong interplanetary field enhancements at Ulysses. Icarus 166, 297–310.

Kempf, S., Srama, R., Altobelli, N., Auer, S., Tschernjawski, V., Bradley, J., Burton, M.E., Helfert, S., Johnson, T.V., Krüger, H., Moragas-Klostermeyer, G., Grün, E., 2004. Cassini between Earth and asteroid belt: first in-situ charge measurements of interplanetary grains. Icarus 171, 317–335.

Kempf, S., Srama, R., Horanyi, M., Burton, M.E., Helfert, S., Moragas-Klostermeyer, G., Roy, G., Grün, E., 2005. High-velocity streams of dust originating from Saturn. Nature 433, 289–291.

Krüger, H., Grün, E., Hamilton, D.P., Baguhl, M., Dermott, S.F., Fechtig, H., Gustafson, B.A., Hanner, M.S., Horányi, M., Kissel, J., Lindblad, B.A., Linkert, D., Linkert, G., Mann, I., McDonnell, J.A.M., Morfill, G.E., Polanskey, C., Riemann, R., Schwehm, G.H., Srama, R., Zook, H.A., 1999a. Three years of Galileo dust data: II. 1993 to 1995. Planetary Space Sci. 47, 85–106 Paper IV.

Krüger, H., Grün, E., Landgraf, M., Baguhl, M., Dermott, S.F., Fechtig, H., Gustafson, B.A., Hamilton, D.P., Hanner, M.S., Horányi, M., Kissel, J., Lindblad, B., Linkert, D., Linkert, G., Mann, I., McDonnell, J.A.M., Morfill, G.E., Polanskey, C., Schwehm, G.H., Srama, R., Zook, H.A., 1999b. Three years of Ulysses dust data: 1993 to 1995. Planetary Space Sci. 47, 363–383 Paper V.

Krüger, H., Grün, E., Graps, A.L., Bindschadler, D.L., Dermott, S.F., Fechtig, H., Gustafson, B.A., Hamilton, D.P., Hanner, M.S., Horányi, M., Kissel, J., Lindblad, B., Linkert, D., Linkert, G., Mann, I., McDonnell, J.A.M., Morfill, G.E., Polanskey, C., Schwehm, G.H., Srama, R., Zook, H.A., 2001a. One year of Galileo dust data from the jovian system: 1996. Planetary Space Sci. 49, 1285–1301 Paper VI.

Krüger, H., Grün, E., Landgraf, M., Dermott, S.F., Fechtig, H., Gustafson, B.A., Hamilton, D.P., Hanner, M.S., Horányi, M., Kissel, J., Lindblad, B., Linkert, D., Linkert, G., Mann, I., McDonnell, J.A.M., Morfill, G.E., Polanskey, C., HSchwehm, G., Srama, R., Zook, H.A., 2001b. Four years of Ulysses dust data: 1996 to 1999. Planetary Space Sci. 49, 1303–1324 Paper VII.

Krüger, H., Forsyth, R.J., Graps, A.L., Grün, E., 2005a. in: Boufendi, L., Mikikian, M., Shukla, P.K. (Eds.), AIP Conference Proceedings, New Vistas in Dusty Plasmas, pp. 157–160.

Krüger, H., Grün, E., Linkert, D., Linkert, G., Moissl, R., 2005b. Galileo long-term dust monitoring in the jovian magnetosphere. Planetary Space Sci. 53, 1109–1120.

Krüger, H., Bindschadler, D., Dermott, S.F., Fechtig, H., Graps, A.L., Grün, E., Gustafson, B.A., Hamilton, D.P., Hanner, M.S., Horányi, M., Kissel, J., Landgraf, M., Lindblad, B., Linkert, D., Linkert, G., Mann, I., McDonnell, J.A.M., Moissl, R., Morfill, G.E., Polanskey, C., Schwehm, G.H., Srama, R., Zook, H.A., 2006a. Galileo dust data from the jovian system: 1997 to 1999. Planetary Space Sci. in press, Paper VIII.

Krüger, H., Graps, A.L., Hamilton, D.P., Flandes, A., Forsyth, R.J., Horányi, M., Grün, E., 2006b. Ulysses jovian latitude scan of high-velocity dust streams originating from the jovian system. Planetary Space Sci., in press.

Landgraf, M., 2000. Modelling the motion and distribution of interstellar dust inside the heliosphere. J. Geophys. Res. 105 (A5), 10303–10316.

Landgraf, M., Augustsson, K., Grün, E., Gustafson, B.A.S., 1999. Deflection of the local interstellar dust flow by solar radiation pressure. Science 286, 2319–2322.

Landgraf, M., Baggeley, W.J., Grün, E., Krüger, H., Linkert, G., 2000. Aspects of the mass distribution of interstellar dust grains in the solar system from in situ measurements. J. Geophys.Res. 105 (A5), 10343–10352.

Landgraf, M., Krüger, H., Altobelli, N.E.G., 2003. Penetration of the Heliosphere by the interstellar dust stream during solar maximum. J. Geophys. Res. 108, 5–1.

Mann, I., Kimura, H., 2000. Interstellar dust properties derived from mass density mass, distribution, and flux rates in the heliosphere. J. Geophys. Res. 105 (A5), 10317–10328.

Mann, I., Czechowski, A., 2005. Dust destruction and ion formation in the inner solar system. Astrophys. J. Lett. 621, L73–L76.

Mann, I., Grün, E., Wilck, M., 1996. The contribution of asteroid dust to the interplanetary dust cloud: the impact of ULYSSES results on the understanding of dust production in the asteroid belt and of the formation of the IRAS dust bands. Icarus 120, 399–407.

Mann, I., Kimura, H., Biesecker, D.A., Tsurutani, B.T., Grün, E., McKibben, R.B., Liou, J.-C., MacQueen, R.M., Mukai, T., Guhathakurta, M., Lamy, P., 2004. Dust near the sun. Space Sci. Rev. 110, 269–305.

Staubach, P., Grün, E., Jehn, R., 1997. The meteoroid environment near earth. Adv. Space Res. 19, 301–308.

Stone, R.G., Bougeret, J.L., Caldwell, J., Canu, P., de Conchy, Y., Cornilleau-Wehrlin, N., Desch, M.D., Fainberg, J., Goetz, K., Goldstein, M.L., Harvey, C.C., Hoang, S., Howard, R., Kaiser, M.L., Kellogg, P., Klein, B., Knoll, R., Lecacheux, A., Langyel-Frey, D., MacDowall, R.J., Manning, R., Meetre, C.A., Meyer, A., Monge, N., Monson, S., Nicol, G., Reiner, M.J., Steinbert, J.L., Torres, E., de Villedary, C., Wouters, F., Zarka, P., 1992. The unified radio and plasma wave investigation. Astron. Astrophys. Suppl. 92, 291–316.

Svestka, J., Auer, S., Baguhl, M., Grün, E., 1996. in: Gustafson, B.A., Hanner, M.S. (Eds.), Physics, Chemistry and Dynamics of Interplanetary Dust, ASP Conference Series, vol. 104, pp. 481–484.

Taylor, A.D., Baggeley, W.J., Steel, D.I., 1996. Discovery of interstellar dust entering the Earth's atmosphere. Nature 380, 323–325.

Wehry, A., Mann, I., 1999. Identification of β-meteoroids from measurements of the dust detector onboard the Ulysses spacecraft. Astron. Astrophys. 341, 296–303.

Wehry, A., Krüger, H., Grün, E., 2004. Analysis of Ulysses data: radiation pressure effects on dust particles. Astron. Astrophys. 419, 1169–1174.

Wenzel, K., Marsden, R., Page, D., Smith, E., 1992. The Ulysses mission. Astron. Astrophys. Suppl. 92, 207–219.

Willis, M.J., Burchell, M., Cole, M., McDonnell, J.A.M., 2004. Influence of impact ionization detection methods on determination of dust particle flux in space. Planetary Space Sci. 52, 711–725.

Willis, M.J., Burchell, M., Ahrens, T.J., Krüger, H., Grün, E., 2005. Decreased values of cosmic dust number density estimates in the solar system. Icarus 176, 440–452.

Witte, M., Banaszkiewicz, H., Rosenbauer, H., 1996. Recent results on the parameters of interstellar helium from the Ulysses/GAS experiment. Space Sci. Rev. 78 (1/2), 289–296.

Zook, H.A., Grün, E., Baguhl, M., Hamilton, D.P., Linkert, G., Linkert, D., Liou, J.-C., Forsyth, R., Phillips, J.-L., 1996. Solar wind magnetic field bending of Jovian dust trajectories. Science 274, 1501–1503.